62

SATELLITE & MESOMETEOROLOGY
RESEARCH PROJECT

Department of the Geophysical Sciences
The University of Chicago

SPLIT OF A THUNDERSTORM INTO ANTICYCLONIC AND CYCLONIC STORMS AND THEIR MOTION AS DETERMINED FROM NUMERICAL MODEL EXPERIMENTS

by

Tetsuya Fujita and Hector Grandoso

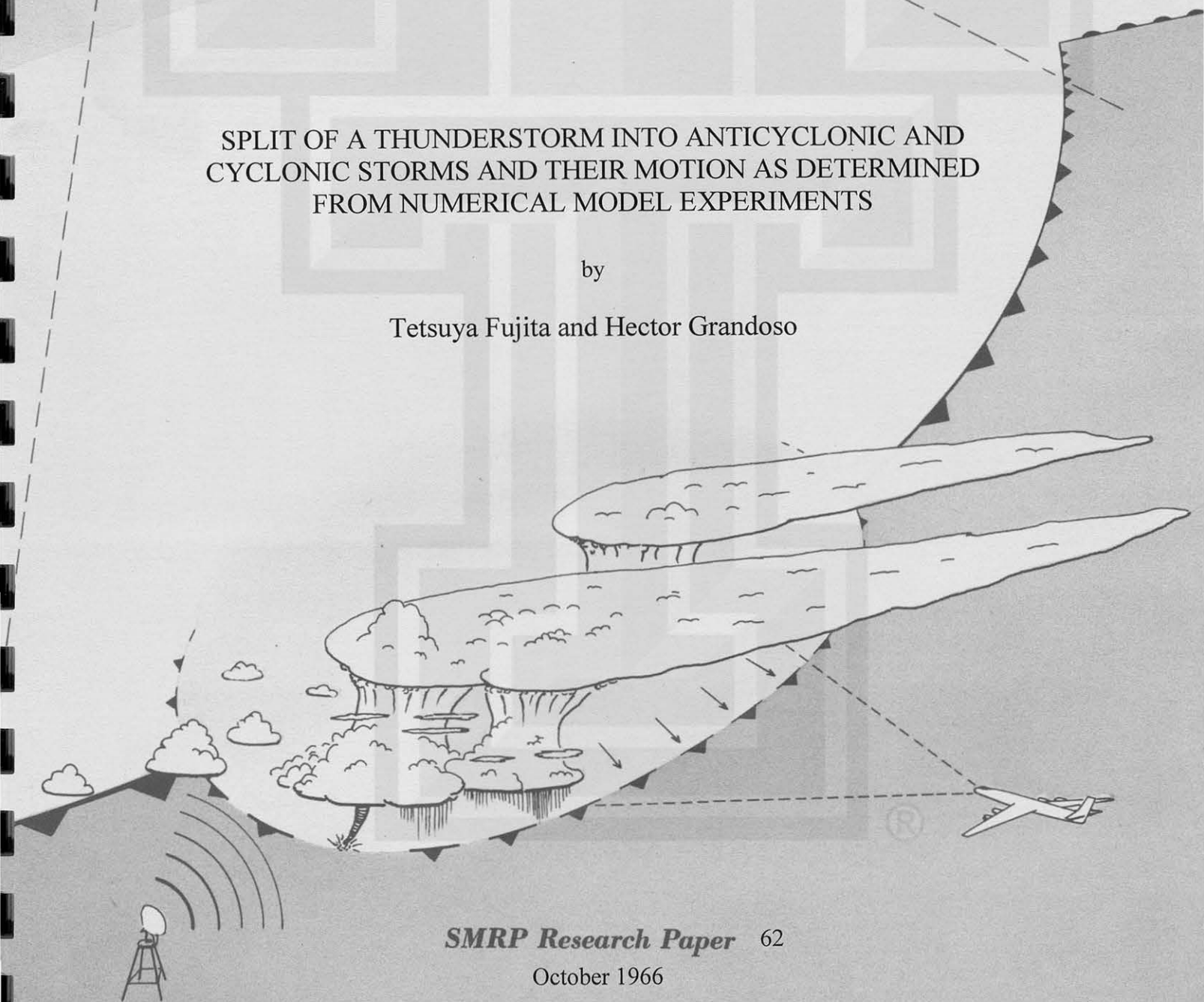

SMRP Research Paper 62

October 1966

MESOMETEOROLOGY PROJECT --- RESEARCH PAPERS

1.* Report on the Chicago Tornado of March 4, 1961 - Rodger A. Brown and Tetsuya Fujita

2.* Index to the NSSP Surface Network - Tetsuya Fujita

3.* Outline of a Technique for Precise Rectification of Satellite Cloud Photographs - Tetsuya Fujita

4.* Horizontal Structure of Mountain Winds - Henry A. Brown

5.* An Investigation of Developmental Processes of the Wake Depression Through Excess Pressure Analysis of Nocturnal Showers - Joseph L. Goldman

6.* Precipitation in the 1960 Flagstaff Mesometeorological Network - Kenneth A. Styber

7.** On a Method of Single- and Dual-Image Photogrammetry of Panoramic Aerial Photographs - Tetsuya Fujita

8. A Review of Researches on Analytical Mesometeorology - Tetsuya Fujita

9. Meteorological Interpretations of Convective Nephsystems Appearing in TIROS Cloud Photographs - Tetsuya Fujita, Toshimitsu Ushijima, William A. Hass, and George T. Dellert, Jr.

10. Study of the Development of Prefrontal Squall-Systems Using NSSP Network Data - Joseph L. Goldman

11. Analysis of Selected Aircraft Data from NSSP Operation, 1962 - Tetsuya Fujita

12. Study of a Long Condensation Trail Photographed by TIROS I - Toshimitsu Ushijima

13. A Technique for Precise Analysis of Satellite Data; Volume I - Photogrammetry (Published as MSL Report No. 14) - Tetsuya Fujita

14. Investigation of a Summer Jet Stream Using TIROS and Aerological Data - Kozo Ninomiya

15. Outline of a Theory and Examples for Precise Analysis of Satellite Radiation Data - Tetsuya Fujita

16. Preliminary Result of Analysis of the Cumulonimbus Cloud of April 21, 1961 - Tetsuya Fujita and James Arnold

17. A Technique for Precise Analysis of Satellite Photographs - Tetsuya Fujita

18. Evaluation of Limb Darkening from TIROS III Radiation Data - S.H.H. Larsen, Tetsuya Fujita, and W.L. Fletcher

19. Synoptic Interpretation of TIROS III Measurements of Infrared Radiation - Finn Pedersen and Tetsuya Fujita

20. TIROS III Measurements of Terrestrial Radiation and Reflected and Scattered Solar Radiation - S.H.H. Larsen, Tetsuya Fujita, and W.L. Fletcher

21. On the Low-level Structure of a Squall Line - Henry A. Brown

22. Thunderstorms and the Low-level Jet - William D. Bonner

23. The Mesoanalysis of an Organized Convective System - Henry A. Brown

24. Preliminary Radar and Photogrammetric Study of the Illinois Tornadoes of April 17 and 22, 1963 - Joseph L. Goldman and Tetsuya Fujita

25. Use of TIROS Pictures for Studies of the Internal Structure of Tropical Storms - Tetsuya Fujita with Rectified Pictures from TIROS I Orbit 125, R/O 128 - Toshimitsu Ushijima

26. An Experiment in the Determination of Geostrophic and Isallobaric Winds from NSSP Pressure Data - William Bonner

27. Proposed Mechanism of Hook Echo Formation - Tetsuya Fujita with a Preliminary Mesosynoptic Analysis of Tornado Cyclone Case of May 26, 1963 - Tetsuya Fujita and Robbi Stuhmer

28. The Decaying Stage of Hurricane Anna of July 1961 as Portrayed by TIROS Cloud Photographs and Infrared Radiation from the Top of the Storm - Tetsuya Fujita and James Arnold

29. A Technique for Precise Analysis of Satellite Data, Volume II - Radiation Analysis, Section 6. Fixed-Position Scanning - Tetsuya Fujita

30. Evaluation of Errors in the Graphical Rectification of Satellite Photographs - Tetsuya Fujita

31. Tables of Scan Nadir and Horizontal Angles - William D. Bonner

32. A Simplified Grid Technique for Determining Scan Lines Generated by the TIROS Scanning Radiometer - James E. Arnold

33. A Study of Cumulus Clouds over the Flagstaff Research Network with the Use of U-2 Photographs - Dorothy L. Bradbury and Tetsuya Fujita

34. The Scanning Printer and Its Application to Detailed Analysis of Satellite Radiation Data - Tetsuya Fujita

35. Synoptic Study of Cold Air Outbreak over the Mediterranean using Satellite Photographs and Radiation Data - Aasmund Rabbe and Tetsuya Fujita

36. Accurate Calibration of Doppler Winds for their use in the Computation of Mesoscale Wind Fields - Tetsuya Fujita

37. Proposed Operation of Intrumented Aircraft for Research on Moisture Fronts and Wake Depressions - Tetsuya Fujita and Dorothy L. Bradbury

38. Statistical and Kinematical Properties of the Low-level Jet Stream - William D. Bonner

39. The Illinois Tornadoes of 17 and 22 April 1963 - Joseph L. Goldman

40. Resolution of the Nimbus High Resolution Infrared Radiometer - Tetsuya Fujita and William R. Bandeen

41. On the Determination of the Exchange Coefficients in Convective Clouds - Rodger A. Brown

* Out of Print
** To be published

(Continued on back cover)

SATELLITE AND MESOMETEOROLOGY RESEARCH PROJECT
Department of the Geophysical Sciences
The University of Chicago

SPLIT OF A THUNDERSTORM INTO ANTICYCLONIC AND CYCLONIC STORMS AND THEIR MOTION AS DETERMINED FROM NUMERICAL MODEL EXPERIMENTS

by

Tetsuya Fujita and Hector Grandoso

SMRP Research Paper #62
October 1966

The research reported in this paper has been sponsored by the National Severe Storms Laboratory, ESSA under Grant Cwb WBG-70.

SPLIT OF A THUNDERSTORM INTO ANTICYCLONIC AND CYCLONIC STORMS AND THEIR MOTION AS DETERMINED FROM NUMERICAL MODEL EXPERIMENTS[1]

Tetsuya Fujita and Hector Grandoso
The University of Chicago

ABSTRACT

Since the concept of a rotational thunderstorm was presented by Byers in 1942, little attention has been paid to this important characteristic. Through direct and indirect observations, as well as a series of numerical experiments, the authors, some 24 years later, now postulate that many large thunderstorms are rotating. The numerical experiments revealed that a thunderstorm in a strong environmental wind field deviates to the left of the mean wind unless it rotates slowly and cyclonically. It was also found that the maximum deviation, either to the right or left, occurs when such a thunderstorm rotates with a critical tangential speed of only a few meters per second. This striking result contradicts the conventional expectation that the faster the rotation, the larger the storm's deviation. Further investigation of numerically-produced clouds, 14,400 in total, revealed that most of the peculiar motion of thunderstorms can be simulated by computing the momentum of clouds through step-by-step integration. A thunderstorm couplet formed by an echo split was successfully simulated numerically. Then the tracks of both cyclonic and anticyclonic storms, almost identical to those observed by radar, were obtained by a computer. The experimental results in comparison with actual storms lead us to conclude that a cloud cannot be treated as a well-mixed entity and that it does not deviate accidentally. Its motion is a consequence of various parameters, including slow rotation, mostly cyclonic but rarely anticyclonic.

---

[1] The research reported in this paper has been sponsored by the National Severe Storms Laboratory, ESSA under Grant Cwb WBG-70.

1. Introduction

Aside from its more violent aspects, no feature of the severe thunderstorm has received more attention in recent research than that of translational motion. This interest is stimulated by observations which show a wide diversity in individual storm paths when upper winds are nearly uniform over a broad area. To date, attempts to account for storm motions which deviate from expected means have centered mainly around the concept of new cloud growth in a preferred storm quadrant. Recently much evidence has been accumulating which suggests that many thunderstorms rotate during their mature stages. Acceptance of this rotational evidence leads to the conclusion that a revision of present physical models of thunderstorms is necessary if we hope to achieve noteworthy progress in the application of dynamical theory.

In his "Physics of the Air", Humphreys (1928) postulated that the velocity of a cloud is usually nearly that of the air in which it floats, and except for the case of a stationary wave-type cloud, meteorologists accepted this simple rule for some time. Early work with weather radar led Ligda (1953) to his definition of SPA winds after his investigations showed that small precipitation echoes tend to move with the wind at the cloud level.

The results of pioneering efforts in the application of radar to the study of thunderstorm motion were reported in "The Thunderstorm" by Byers and Braham (1949). The small single-cell storms with which they dealt were shown to move with the direction of the mean wind from the gradient to 20,000 ft level. They describe an instance, however, when a small echo, originally moving with the direction of the low-level winds, gradually changed its direction to that of the middle-level winds as it increased in height, suggesting that steering forces effected the change in movement.

Operational meteorologists have long been aware that the movement of large radar echoes is sometimes erratic and usually quite different from those of more uniform size. The relationship between converging echoes and the occurrence of severe storms was investigated by Stout and Hiser (1955) and they found that the time and location of the tornado of May 28, 1954 near Peoria, Ill. corresponded to the merger of two echoes which had been on converging tracks.

Using the hourly precipitation records available from more than 2000 rain gages throughout the midwest, Newton and Katz (1958) were able to track large convective rain areas and correlated their motion with mean winds between 850 and 500 mb. Their results indicated that the rainstorms moved with a systematic deviation of about

25° to the right of the mean wind direction. They explained the deviation as a new, successive formation on the right side of the storms and concurrent dissipation on the opposite side. Newton and Newton (1955) further pursued this phenomenon and proposed a convective cloud model that includes the generation of a large vertical hydrodynamic pressure gradient in an area near the edge of the cloud where the stagnation point at low level lies beneath the accelerated flow near the cloud top. Such a gradient would favor a new updraft just outside the cylindrical cloud, assumed to be a completely mixed body or solid cylinder.

Based on the premise that the role of a convective cloud in abstracting relative low-level moist inflow increases with storm diameter, Newton and Fankhauser (1964) investigated the deviation of storm motion as a function of the size of PPI radar echoes. The analytical expression based on moist air continuity which they develop and the empirical samples against which it is tested both show that there is a tendency for larger storms to deviate farther to the right of some mean reference angle (in their case the mean tropospheric wind direction). There remained, however, considerable residual scatter in their data which cannot be explained in terms of water budget considerations and upper winds alone and has led to the cooperative effort by the present authors.

It is not entirely clear when the concept of "rotating thunderstorms" appeared in the early literature. Nonetheless, the remarks on thunderstorm circulation by Byers (1942) should be credited as the earliest attempt to explain the right-veering of thunderstorms, using the so-called "rotor" principle. Some 15 years later, Fujita (1958) revealed that the parent thunderstorm that produced the Illinois tornadoes of April 9, 1953 was located inside a tornado cyclone which traveled in a direction about 25° to the right of the general flow. At that time he did not attempt to explain the motion of the rotating wind system.

Independent studies of the tornadic storms of May 26, 1963 by Browning (1965a, 1965b) and Fujita (1965) have helped to clarify various aspects of storms characterized by so-called hook echoes. Browning attempted to estimate the movement and trajectories of hydrometeors within the storms, which veered almost 40° to the right. The term "vault," introduced earlier by Browning (1964), was applied to the explanation of echo-free, but supposedly cloud-packed regions, of suspected intense updraft. In contrast with Browning's emphasis, Fujita extended some earlier work on mesocyclones [Fujita (1963)] and analyzed the same case based upon the assumption that an echo with a hook is accompanied by circulation.

He then pointed out the existence of an eye around the rotation axis which was supposed to be both echo- and cloud-free when fully developed. The magnus lift force was introduced as a cause of the significant right-veering of the storms, and it was pointed out that if such a steering mechanism is important, a left-veering anticyclonic storm could also be predicted.

Browning's comment and Fujita's reply (1965) clarified various points which could be raised by severe storms' researchers. The clear distinction between Browning's "vault" and Fujita's "eye", in particular, was one of the focal points brought up in the correspondence. It was pointed out that both of these echo-free features may co-exist within the same cloud, but the dynamical aspects of the areas of the vault and the eye are entirely different from each other.

In order to further pursue research regarding dynamical structure of thunderstorms which may or may not be rotating, it has become necessary to determine the flow patterns around isolated thunderstorms at various levels. Since airborne Doppler-wind systems are most suitable at the present time for horizontal-wind sampling around isolated storms, an estimate of their accuracy and the subsequent correction of possible errors was undertaken in great detail by Fujita (1966) and Fujita, Black, and Loesch (1966). As a result of these investigations, controlled flight patterns to minimize wind errors and an accurate error-correction method have been devised, making it possible to utilize airborne Doppler winds in the determination of mesoscale wind fields around isolated clouds.

This paper presents the latest results of the Doppler-measured flow patterns around clouds and the dynamical evaluation of the interacting forces between the clouds and the ambient atmosphere. The clouds are then treated as a drifting entity in the atmosphere, leading to numerical experiments of the vertical transport of momentum under the influence of a vertical wind shear. The implications of these numerical experiments are drawn on to help explain the phenomenon of splitting thunderstorms which have been found recently in radar data gathered by the National Severe Storms Laboratory, Norman, Okla. An initial echo is observed to separate and form two entities, one on the right which veers markedly to the right of the presplit trajectory and one on the left which veers clearly to the left. The angle between the directions of the two new elements is as large as 60°.

2. Drag Coefficient of Isolated Cumulonimbus

A large cumulonimbus cloud embedded in a strong wind acts to a certain extent as an obstacle even though its behavior is somewhat different from that of a solid chimney blocking the flow. First, the cloud moves under the influence of the drag and the Coriolis forces, while the vertical transport of momentum continuously counteracts these forces so that a cloud with significant updraft always maintains its own velocity, differing from that of the environmental atmosphere. Second, the side of the cloud is continuously eroded through entrainment processes which stimulate the eddy transfer of momentum between incloud and environmental air.

The order of magnitude of the Reynolds number for cumulonimbus clouds obtained from

$$R = \frac{UD}{\nu} \quad ,$$

where ν represents the kinematic viscosity, U, the relative wind speed, and D, the cloud diameter, would be extremely large. For example, when U = 10 m/sec and D = 10 km, the Reynolds number is of the order of 10^9, which is way above the critical Reynolds number of a solid cylinder. It is expected, therefore, that the drag coefficient of such a cloud would be about 0.3, according to Wieselsberger (1921), who measured the resistances of cylinders of various diameters at various flow velocities.

Direct measurements of the drag coefficient of a cumulonimbus do not seem to be plausible at the present time. Yet to estimate it from the Reynolds number and Wieselberger's measurements may not be reliable in view of the fact that kinematic eddy viscosity is more appropriate than kinematic viscosity in determining the flow regime around a cumulonimbus. Since the former viscosity is several orders of magnitude larger than the latter, the use of the former could result in a Reynolds number below the critical value.

The resistance of a body in viscous fluid can be calculated from momentum considerations which do not require direct measurements of forces. Prandtl and Tietjens (1934) derived a simple method of computing the resistance of a body from the velocity distribution in the wake flow. The method is applicable to a cloud if the

wind field around the cloud is obtained by an airborne Doppler wind system. To make computation easier, we assume that the airplane flies at a constant pressure surface. Expressing the undisturbed wind relative to the cloud by U, a constant, and the relative wind in the wake flow by U_w, we write the difference in the momentum flowing into and out from the layer of unit thickness per unit time as

$$\underset{\text{(goes in)}}{\rho\int U^2 dy} - \underset{\text{(goes out)}}{\rho\int U_w^2 dy} = \rho\left[\int U^2 dy - \int U^2 dy + 2\int U\Delta U\, dy - \int \Delta U^2 dy\right], \quad (1)$$

where $\Delta U = U - U_w$; ρ, the density; and y, the length in the direction perpendicular to the undisturbed flow. This difference in the momentum is equal to the resistance of the cloud upon the layer of unit thickness. Using the conventional expression of the resistance force, we write

$$C_D D \tfrac{1}{2}\rho U^2 = 2\rho\int U\Delta U\, dy - \rho\int \Delta U^2 dy ,$$

where C_D denotes the drag coefficient and D the diameter of the cloud. When the wind inside the wake is measured far away from the cloud, ΔU^2 can be neglected. Thus we have

$$\tfrac{1}{2} C_D D U = 2\int \Delta U\, dy . \quad (2)$$

The drag coefficient of the cloud is now written as

$$C_D = \frac{4}{DU}\int \Delta U\, dy . \quad (3)$$

In order to determine the drag coefficient of a cloud, an isolated thunderstorm of April 21, 1961 was selected because of the availability of measured Doppler winds at three levels all around the cloud. In fact, a picture of this cloud appeared as the cover photograph of the AMS Bulletin, April 1965. The results of preliminary analyses had already been reported by Fujita and Arnold (1963) and Fujita (1963). Shown in Fig. 1 is the field of Doppler winds relative to the cloud moving at 22 kt from the direction, 268°. Because the cloud was rotating cyclonically, the axis of the wake flow extending from the rear stagnation point is a curved line. Nevertheless, the wake flow, characterized by relatively weak winds, was depicted in two traverses through the wake some 40 and 70 km downwind from the cloud. Drag coefficients computed from Eq. (3) with D = 10 km, U = 12 m/sec are $C_D = 1.0 \pm 0.2$ for Traverse 1 and $C_D = 1.1 \pm 0.2$ for Traverse 2.

This cumulonimbus was accompanied by a 6 m/sec rotational wind speed around the 30-km diameter. The circulation was, therefore,

$$\Gamma = \pi D V_{30} \cong 56 \times 10^8 \ \text{cm}^2/\text{sec}, \qquad (4)$$

where Γ denotes the circulation; D, the diameter; and V_{30}, the rotational speed at D = 30 km. Under the assumption that the flow is irrotational outside the core of 10-km diameter, the rotational speed at the rim of the core is estimated to be V_{10} = 18 m/sec. Thus the ratio of the rotational and the translational speeds turns out to be

$$V/U = 18/12 = 1.5.$$

Experimental results by Prandtl and Tietjens (1934), transcribed in Fig. 2, indicate that the drag coefficient of a rotating cylinder remains practically the same as long as the V/U ratio is less than about three. For the purpose of estimating the drag coefficient of a rotating cloud, we may thus assume that a cloud is not rotating. Using these estimated values, the wind field in Fig. 1 will be re-examined. The isotachs in dashed lines represent the relative wind speeds. A 57-kt speed is seen to the right of the cloud which was rotating cyclonically. Both cyclonic and anticyclonic vortices, designated by letters "C" and "A," are schematically drawn on the downwind side of the cloud. These vortices probably drift away from the cloud, thus producing either a Kármán or an irregular vortex trail.

An enlargement of the relative flow pattern in the vicinity of the cloud appears in Fig. 3, in which winds are plotted at 20-sec intervals from the Doppler winds measured at one-second intervals. The flow patterns as well as the wind-speed profiles across the upwind and downwind streams clearly indicate that the cloud acted as an obstacle, forcing the environmental flow to go around it.

3. Forces Acting upon a Rotating Cloud under the Influence of Drag Force and Entrainment

Since a cloud is far from a solid cylinder standing on the ground, it must move under the influence of various forces. At the same time, the entrainment at the edge of the cloud initiates momentum exchange between the cloud and its environment through eddy transport processes. When the relative winds are very strong, a considerable amount of mass is carried away from the cloud, thus necessitating the use of eddy viscosity. In order to overcome difficulties in the mathematical solution of the problem, four forces acting upon a rotating cloud will first be considered (Fig. 4). These forces per unit mass of cloud within the layer of unit thickness are listed as follows:

(1) Gradient force per unit cloud mass,

$$\mathbf{F}_G = -\frac{1}{\rho}\nabla P = -f\,\mathbf{W}\times\hat{\mathbf{k}}\ , \qquad (5)$$

where $\mathbf{W}$ denotes the geostrophic wind velocity; $\hat{\mathbf{k}}$, the unit vector toward the zenith; and other symbols represent conventional expressions.

(2) Coriolis force per unit cloud mass,

$$\mathbf{F}_c = f\mathbf{S} \times \hat{\mathbf{k}} \quad , \tag{6}$$

where $\mathbf{S}$ is the velocity of the storm.

(3) Drag force per unit cloud mass,

$$\mathbf{F}_D = \frac{2}{\pi D} C_D U^2 \hat{\mathbf{r}} \quad , \tag{7}$$

where U is the relative wind blowing toward the unit vector, $\hat{\mathbf{r}}$; and C_D, the drag coefficient.

(4) Lift force per unit mass of a rotating cloud,

$$\mathbf{F}_L = \frac{2}{\pi D} C_L U^2 \hat{\mathbf{r}} \times \hat{\mathbf{k}} \quad , \tag{8}$$

where C_L denotes the lift coefficient.

When these four forces are added vectorially, it is seen that the gradient, Coriolis, and lift forces are in the direction perpendicular to the relative wind. Thus we write

$$\mathbf{F} = \mathbf{F}_G + \mathbf{F}_C + \mathbf{F}_D + \mathbf{F}_L = \left(\frac{2}{\pi D} C_L U^2 - f U\right) \hat{\mathbf{r}} \times \hat{\mathbf{k}} + \frac{2}{\pi D} C_D U^2 \hat{\mathbf{r}}$$

$$= \frac{2}{\pi D}\left\{\left(C_L U^2 - \frac{\pi D}{2} f U\right) \hat{\mathbf{r}} \times \hat{\mathbf{k}} + C_D U^2 \hat{\mathbf{r}}\right\} \quad . \tag{9}$$

The absolute value of $\mathbf{F}$ and its azimuth measured from $\mathbf{U} = U\hat{\mathbf{r}}$ are, therefore,

$$F = \frac{2}{\pi D}\left\{\left(C_L U^2 - \tfrac{1}{2}\pi D f U\right)^2 + C_D^2 U^4\right\}^{\frac{1}{2}} \tag{10}$$

and

$$\theta = \tan^{-1} \frac{C_L U^2 - \frac{1}{2}\pi D f U}{C_D U^2} \quad , \tag{11}$$

respectively.

These equations include drag and lift coefficients. If we generalize the drag coefficient discussed in the previous section, we may assume that $C_D \cong 1$, and the Reynolds number applicable to the flow around a large cloud would still be below the critical Reynolds number.

The lift coefficient from the lift formula by Kutta-Joukowsky includes the ratio of rotational and relative wind speeds, thus

$$C_{L(K-J)} = 2\pi\left(\frac{V}{U}\right) . \qquad (12)$$

Through experiment, however, the lift coefficient can be obtained in the form of

$$C = \text{Function}\left(\frac{V}{U}\right) . \qquad (13)$$

In order to compare the lift coefficients given by Eqs. (12) and (13), Fig. 2 was prepared. It should be noted that these coefficients are negative when a cloud rotates anticyclonically, or V is negative. The figure indicates that the Kutta-Joukowsky lift coefficient increases in proportion to the rotation rate of a cloud. The experimental coefficient obtained by Prandtl, on the other hand, is very small until the rotational speed approaches the relative wind speed, suggesting that the effect of the cloud rotation upon the lift force is relatively small when a cloud rotates slowly.

Even for a large cumulonimbus cloud, the effect of entrainment cannot be entirely neglected. In order to estimate the amount of entrainment as the incloud air rises, we assume that the ambient air first entrains through the cloud boundary and mixes with the uprising air, forming a large number of turbulent eddies. This process of mixing the incloud and the ambient air also involves the mixing of the horizontal momentum which will be considerably larger than that of the incloud air. As a result, they will be eroded away into the wake region. This erosion will become significant when a cloud is influenced by a strong vertical wind shear. From these considerations, we assume that the cloud loses the same amount of air that entrains through its boundary; that is, the entrainment is regarded as "detrainment."

Entrainment will thus increase the total mass of a cloud when the entrained air stays in the cloud or it will reduce the mass of undiluted rising air when erosion takes place. After defining the vertical mass transport through a constant pressure surface or through a constant geopotential surface,

$$M = \frac{\pi}{4} D^2 \rho w \qquad (14)$$

we use the result of Fujita's (1963) summary that entrainment is inversely proportional to the cloud diameter, D, and write

$$\frac{dM}{M}\Big/_{dp} = \mp k_p D^{-1} \qquad (+ \text{ for erosion}) \qquad (15)$$

and

$$\frac{dM}{M}\Big/_{dz} = \pm k_z D^{-1} \qquad (- \text{ for erosion}) \qquad (16)$$

where k_p is assumed as a constant when entrainment is defined by Eq. (15) and k_z, another constant when defined by Eq. (16). It should be noted that k_p and k_z cannot be constants simultaneously, since dp and dz are related hydrostatically by $dp = -\rho g dz$. In reality, however, both k_p and k_z will vary as a function of either pressure or height. For computational purposes when using adiabatic charts, it is convenient to assume that k_p is constant, so that the thermodynamical properties of the mixed air can be computed as a function of pressure.

To make our computation easier, we define entrainment by Eq. (16), then determine the constant from the approximate values, $dM/M = 0.06$, $dz = 1.5$ km, and $D = 10$ km, from Fujita's (1963) summary, thus

$$k_z = \left| \frac{D}{M} \frac{dM}{dz} \right| = 0.4 . \qquad (17)$$

We shall now compute the diameter of the undiluted incloud air as a function of height, assuming that the density of the air, ρ, and the vertical velocity of the rising air, w, are known, respectively, as functions of height. First we differentiate Eq. (14) after taking the natural logarithm and combine the result with Eq. (16) to obtain

$$2\,dD + D\,d(\ln \rho w) = -k_z\,dz .$$

By introducing a function,

$$F = \frac{d(\ln \rho w)}{dz}$$

this equation can be written in the form of

$$\frac{dD}{dz} + \frac{F_z}{2} D = -\frac{1}{2} k_z . \qquad (18)$$

It is evident that this differential equation can be solved as long as k_z is given as a function of z. The integrating factor of this equation is thus given by

$$I = e^{\frac{1}{2}\int F_z dz} = e^{\frac{1}{2}\ln \rho w} = (\rho w)^{\frac{1}{2}} .$$

The solution of Eq. (18) is now expressed in a simple form,

$$D = (\rho w)^{-\frac{1}{2}} \left[-\frac{1}{2} \int k_z (\rho w)^{\frac{1}{2}}\, dz + c \right] ,$$

where the integrating constant is determined by putting the initial conditions at the cloud base, $D = D_o$, $\rho = \rho_o$, and $w = w_o$. Thus we write the final solution,

$$D = \left(\frac{\rho_o w_o}{\rho w}\right)^{\frac{1}{2}} D_o - \frac{1}{2}(\rho w)^{-\frac{1}{2}} \int_{h_o}^{h} k_z (\rho w)^{\frac{1}{2}} \, dz \,, \qquad (19)$$

where D represents the diameter of the undiluted cloud at height, h, and h_o, the height of the cloud base. It should be noted that each of these three parameters, ρ, w, and k_z, in Eq. (19) is assumed to vary with height.

In a special case when k_z is constant, the solution is reduced to

$$D = \left(\frac{\rho_o w_o}{\rho w}\right)^{\frac{1}{2}} D_o - \frac{1}{2} k_z (\rho w)^{-\frac{1}{2}} \int_{h_o}^{h} (\rho w)^{\frac{1}{2}} \, dz \,.$$

The first term on the right side of this solution denotes the change in the cloud diameter due to continuity, but the second term represents the reduction of the diameter as a result of erosion around the edge of the undiluted air. It is seen that the diameter of the undiluted core may become zero, especially when D_o is small [2], thus prohibiting the growth of a cloud as high as the tropopause.

As a result of entrainment followed by detrainment and erosion processes around the side of a cloud, the circulation around a cloud, Γ, decreases with height. In computing the vertical distribution of Γ, we assume that the undiluted core rotates at the angular velocity computed under the assumption of no entrainment. Therefore, the loss of circulation is entirely caused by erosion processes in which the cloud loses the mass around the periphery having high rotational speed. From the conservation

---

[2] If ρw is constant, for instance, Eq. (19) can immediately be integrated into

$$D = D_o - \frac{1}{2} k_z (h - h_o)$$
$$\cong D_o - 0.2 (h - h_o)$$

by using the approximate value of k_z given in Eq. (17). In such a case, the undiluted core would disappear at the height,

$$h_m - h_o \cong 5 D_o ,$$

where h_m denotes the maximum height of the undiluted core. This result suggests that D_o must be more than about three miles if the core is expected to reach the tropopause.

Further discussion on the change in D as a function height under various entrainment coefficients appears in the Appendix 1.

of mass and circulation, we write

$$\pi D_c V_c = \Gamma_o \quad \text{and} \quad \frac{\pi}{4} D_c^2 \rho w = M_o ,$$

where the suffix "c" denotes the values representing the conservation case. The angular velocity in the conservation case,

$$\Omega_c = \frac{2V_c}{D_c} = \frac{\Gamma_o}{2M_o} \rho w , \qquad (20)$$

is now applied to the rotation rate of the eroded core to obtain Γ, the circulation around the undiluted core,

$$\Gamma = \frac{1}{2} \pi D^2 \Omega_c = \frac{\pi \Gamma_o}{4M_o} \rho w D^2 \qquad (21)$$

where the diameter, D, is computed from Eq. (19), using ρ, w, and k_z. The rotational speed or the tangential speed around the core can now be given by

$$V = \frac{\Gamma_o}{4M_o} \rho w D . \qquad (22)$$

4. Three-dimensional Features and Motion of Rotating Thunderstorms

Mathematical solutions of the forces discussed in the preceding section were based upon the assumption that the incloud air rises from the base of the cloud, while entrainment processes continuously mix ambient and incloud air around the periphery of the rising air and the mixed air is eroded away into the wake. The cloud in this model is defined as the undiluted portion of the cloud core which may rotate in either a cyclonic or anticyclonic sense. The mass transport inside the core, as well as the circulation, is therefore considered to decrease with the height.

In order to obtain three-dimensional features and the motion of a cloud developing under various wind shear, we consider that the ambient wind, $\mathbf{W}$, air density, ρ, and the vertical velocity, w, are known, respectively, as functions of height. The basic problem involved in the step-by-step calculation for the determination of the horizontal displacement of incloud drafts was first discussed by Bates (1961), leading to his "wafer method." In order to obtain the horizontal acceleration of the indraft air, Bates sliced a draft into a stack of wafers with uniform draft velocity in each wafer. Then he applied the aerodynamic drag caused by the velocity difference between

the ambient and the indraft air.

The wafer method was not applied to the solution of hydrodynamic problems involving clouds for several years, until Bates and Newton (1965) made an attempt to compute the two-dimensional trajectories of draft wafers rising from the base of a cloud moving with a translational velocity considered different from the horizontal speed of the wafer at the foot of the draft. They more or less considered that the arrival of a cloud above a given point initiates or triggers a draft wafer to rise from that point. After the draft wafer starts rising, they assumed that the wafer moves under the influence of the drag force computed as a function of the relative velocity between the wafer and the ambient air. Their approach to the solution of the three-dimensional structure of incloud drafts is imaginative and interesting. Nevertheless, its application to actual up- and downdrafts needs to be improved, since the drag force acting upon an incloud draft should be a function of the relative velocity between the draft wafer and the incloud air, not the ambient air.

In order to avoid the above-mentioned difficulties involving the velocities of ambient, incloud and indraft air, our mathematical solutions are limited to the interaction between incloud and ambient air. The velocity of a cloud is thus defined as

$$\int_{h_o}^{h_t} \frac{\pi}{4} \rho D^2 \mathbf{S}\, dz \quad = \quad \overline{\mathbf{S}} \int_{h_o}^{h_t} \frac{\pi}{4} \rho D^2\, dz \ , \qquad (23)$$

where $\overline{\mathbf{S}}$ denotes the velocity of a cloud if its entire mass were brought together into a point mass without changing the total horizontal momentum of the cloud. The integration in Eq. (23) is performed from the height of the cloud base, h_o, to the cloud top, h_t. The velocity thus defined is called the "inertia velocity"[3] of a storm. Because the inertia velocity is proportional to the horizontal momentum of a storm, it could be different from the "translational velocity," which is also affected by new storm development in a preferable quadrant of a traveling storm. Newton and Fankhauser (1964) demonstrated the effect of such development upon the echo movement.

In order to apply a step-by-step integration method in the computation of the horizontal velocity of the undiluted incloud air, a cloud is sliced into circular discs of uniform thickness, Δz (Fig. 5). Then we assign a suffix "o" to the parameters at the lowest layer, which are $\mathbf{W}_o$ (vector), ρ_o, w_o, $\mathbf{S}_o = \mathbf{W}_o$, M_o, and Γ_o. In addition to these, $\mathbf{W}$, ρ, and w are also given for use as input data. We then compute

---

[2] The shape of the model cloud in relation to inertia velocity is described in Appendix II.

1. Cloud diameter, D, from D_o, ρ, ρ_o, w, w_o, and k_z, using Eq. (19).
2. Rotational velocity, V, from Γ_o, M_o, w, D, ρ, and Eq. (22).

At this point it becomes necessary to obtain the velocities, **S** and **U**, through step-by-step calculation from the cloud base upward. A vector diagram in Fig. 6 is used in determining the horizontal acceleration,

$$\Delta S_n = F_n \Delta t_n = \frac{1}{w_n} F_n \Delta z \quad , \tag{24}$$

where the suffix "n" indicates the quantities in the nth layer and Δt_n, the time required for the rising air to travel through that layer. Even though the vectorial computations of successive velocities are time-consuming, they can be accomplished by expressing the azimuths of three basic vectors, **W**, **S**, and **U**, by α, β, and γ, respectively, and solving the vector triangles. Thus

$$U_n^2 = S_n^2 + W_n^2 - 2S_nW_n \cos\delta_n$$
$$\text{and} \quad \sin\zeta_n = S_n U_n^{-1} \sin\delta_n \tag{25}$$

where $\delta_n = \beta_n - \alpha_n$ and $\zeta_n = \alpha_n - \gamma_n$.

After computing U_n and γ_n from Eq. (25), the direction, θ_n, and the magnitude, F_n, of the resultant forces acting upon the unit mass of undiluted cloud are obtained from Eqs. (10) and (11). We solve the smaller vector triangle in Fig. 6, thus

$$\epsilon_n = \theta_n - \delta_n - \zeta_n \quad ,$$
$$S_{n+1}^2 = S_n^2 + \Delta S_n^2 + 2S_n\Delta S_n \cos\epsilon_n \quad ,$$
$$\text{and} \quad \sin\Delta\beta_n = \frac{\Delta S_n}{S_{n+1}} \sin\epsilon_n \quad , \tag{26}$$

where the suffix "n + 1" refers to the quantities in the (n + 1) layer. From the relation,

$$\beta_{n+1} = \beta_n + \Delta\beta_n \quad ,$$

we finally determine the cloud velocity, **S**, in the layer, n + 1. The computations leading to the determination of S_{n+2} are then repeated until the cloud velocity at the top layer is determined.

One Thousand and Eight Model Clouds

For the purpose of obtaining the features and movement of clouds developing under various vertical wind shears, the height of the base and the top of all clouds are assumed as h_o = 1.5 km and h_t = 12 km, respectively. The cloud was then

sliced into 105 thin discs, each with ρ, the density of the standard atmosphere. The basic parameters used to produce different clouds were selected as follows:

The entrainment coefficient: $k_z = 0.4$ was assumed (refer to the Appendix).

Three w_{max} : cloud I (5 m/s), II (10), and III (15). [4]

Seven V_o : cloud +Fast (+10 m/s), +Medium (+5), +Slow (+2), all cyclonic; cloud -Fast (-10 m/s), -Medium (-5), -Slow (-2), all anticyclonic; and Neutral, a non-rotating cloud.

Four D_o: cloud Small (5 km), Medium (10 and 20), and Giant (40).

Six W: High, Moderate, and Low shears for each of the speed and velocity shear cases.

Two Magnus forces: Prandtl's experimental lift coefficient and Kutta-Joukowsky's lift coefficient.

These parameters would produce a combination of 1008 clouds, thus resulting in a "who's who" of thunderstorms.

It is not the scope of this paper to discuss the features of all clouds. However, the influence of cloud rotation upon their features and movement, obtained through this calculation, will be discussed in the following sections in comparison with the characteristics of actual thunderstorms. Thus the computer model and the actual storm can be effectively compared for verification purposes.

5. Evidences of Splitting Echoes and their Motion after Split

Since Newton and Fankhauser (1964) pointed out an unexplainable motion of an echo on May 24, 1962 which traveled some 30° to the left of the mean wind, questions have been raised as to the predictability of echo motion when such an echo is involved. Then, on April 3, 1964, an extremely complicated echo motion was observed on the WSR-57 radarscope at the National Severe Storms Laboratory at Norman.

---

[4] The vertical velocity used in this model was computed from

$$w = 0.91\, w_{max}\left\{\sin 180h/h_t - \frac{1}{4}\sin 360h/h_t\right\}$$

where h_t denotes the cloud-top height. This formula results in the maximum vertical velocity at 7.4 km above the surface.

The whole event started when a small echo, about 100 nm southwest of the station, suddenly split into two, the one to the right veering about 20° to the right and the other veering over 30° to the left from the direction of echo motion before the split. After making a time-lapse movie from scope pictures taken with identical gain and elevation angles, Wilk (1966) studied this phenomenon in relation to the predictability of severe thunderstorms. In fact, the right-hand storm produced damaging tornadoes near Wichita Falls, Texas and the other left a long swath of 3- to 3 1/4-inch hail.

A very similar situation that developed on May 27, 1965 was studied by Harrold (1966) in order to explain the reasons for the veering of the storms 30° to the left and also 30° to the right in his case. Harrold applied the Kutta-Joukowsky force in the manner suggested by Byers (1942) and Fujita (1965) in order to estimate the ratio,

$$\frac{\text{K-J force}}{\text{drag force}} = \frac{\pi \rho UVDH}{\frac{1}{2}\rho U^2 DH} = \frac{2\pi V}{U}$$

where H denotes the height of a cylinder of diameter, D, and the other symbols have the same designations used in this paper. After putting U = 50 kt and V = 2.5 kt into this formula, he obtained the ratio of 0.3, which would deviate the direction of the resultant force as much as 15° from that of U. Then he assumed that the storm travels toward the direction of this force. From this assumption he concluded that the deviation is only half that observed in his case and that the right-hand storm deviated more toward the region of moisture supply. This however still does not explain in full why the other storm veered to the left.

There are two basic difficulties in accepting Harrold's conclusion, even if we assume that a cloud is a rotating cylinder moving under the influence of the resultant force. (1) The angle of 15° quoted by him is the angle between the force and the relative wind, and the latter is the vector difference between the velocities of the storm and the environmental wind. The vector change in the relative wind will probably reduce this angle to a certain extent. (2) The lack of explanation of the estimated V = 2.5 kt may raise questions as to more reasonable values. Since the isolated cloud of April 21, 1961 was accompanied by V = 12 kt around a 30-km diameter (cf Section 2), Harrold's estimated value could be far below the rotation rate of a thunderstorm of this category. The rotational speed which would result in a 30° angle when computed from his formula is only about 4.5 kt.

In the light of this discussion regarding the phenomenon of echo split and the veering of the echo couplet, it should be realized that the problems involved are rather

complicated. It is unlikely that the horizontal motion of rotating clouds can be estimated by means of a simple guess, which usually fails when too many independent parameters, such as cloud diameter, vertical velocity, wind shear, rotation rate, etc., are involved. If all parameters are taken into consideration, it would become impossible to simulate numerical integrations which nature performs without using electronic computers. Nevertheless, the results of the numerical experiments outlined in the previous section were found to be very useful in the explanation of this phenomenon, thus providing an opportunity to compare the results of a calculated guess and a reasonable one.

In order to further clarify the features and movement of a split-echo couplet, hourly positions of echoes from WSR-57 at NSSL are presented in Fig. 7. The initial echo was moving toward the radar at Norman (NRO) prior to its split at about 1335. The split cell to the right immediately started veering to the right and the other deviated to the left. The angle between the direction of motion of these diverging echoes, initially about 50°, was increased beyond 60° after two to three hours. Winds aloft from Oklahoma City give no indication of tropospheric winds which would steer one of the storms toward the north. Since the major cause of such veerings is related to the sign of the rotational speed of the incloud air, the storm which veered to the right and the other which veered to the left are tentatively identified as "cyclonic storm" and "anticyclonic storm," respectively.

Careful studies of PPI-scope pictures of the storms of April 3, 1966 by the authors revealed that the storm in question split "several" times. When the tracks of the echoes produced by these "multiple splits" were plotted in Fig. 8, they appeared somewhat like the tracks of particles photographed by the Wilson cloud chamber. The sequence of the split occurred after the initial echo, N_0, split into A_1 (anticyclonic) and C_1 (cyclonic) at 1340 CST. Two hours and 40 min later, A_1 split into A_3 and C_3, followed by a split of C_3 into A_4 and C_4 two hours and 50 min later. While these splits were going on, the storm, C_1, split into C_2 and A_2, and they traveled as a couplet toward the region of a newly-forming cyclonic storm, C. Shortly after 1600 CST, the speed of C_2 accelerated considerably toward the southeastern sector of C until the former was captured by the latter. The anticyclonic storm, A_2, was also captured by C shortly before 1700 CST.

One of the most interesting phenomena observed in the vicinity of Storm C is the interaction between C and N, a neutral storm pulled into the southeast quarter of C. Due to proper timing involving their relative motion, a "near-miss" situation

took place, thus allowing N to cross the track of C about 20 min earlier. When this neutral echo was examined after its near-miss crossing, convincing evidence of anticyclonic rotation was noticed on the PPI photographs of the NSSL radar.

Hourly analysis of surface winds from the NSSL Beta Network revealed significant features in the flow pattern over the area of splitting echoes. One of the hourly surface charts is presented in Fig. 9. It will be found that the surface wind fields beneath Storms A_1 and C_2 are characterized, respectively, by definite anticyclonic and cyclonic circulations when tangential wind speeds are integrated along circles 20 to 40 mi in diameter, including the area of this echo couplet. The anticyclonic storm, A_2, located deep inside the mesohigh, was in its dissipating stage, being pulled toward a newly developing storm, C. It should be noted that Storm C was located over jet-like surface winds blowing into the mesohigh with an open entrance along its northeast boundary. Due to the horizontal pressure gradient inside the mesohigh, the jet-like wind diverged toward the north and also toward the southeast boundary where Storms A_1 and C_2 are located. A series of surface charts, such as this example, indicated the existence of a field of circulation in the surface winds beneath each rotating cloud. The circulation was positive beneath all storms veering to the right and negative beneath others veering to the left of the mean wind. Moreover, each storm traveled with a wind-shift line of its own, at least during the period of its mature stage. This evidence suggests that the incloud air rising through the base of a rotating cloud is characterized by a circulation required to keep the cloud rotating and that the cloud carries a proper wind-shift line with it. As a result, a built-in feedback system of angular momentum can be operated with the addition of the relatively small circulation provided by the jet-like surface wind field, which does not always propagate with the velocity of a specific storm. It is postulated that the long life of rotating storms, such as $A_1 + A_3$ (5hr), $C_3 + C_4$ (5hr), and C (4.5hr), is due to this feedback system.

An anticyclonic storm of April 23, 1964 traveled over the western part of the Beta Network, thus providing useful data relating surface flow patterns with both PPI and RHI photographs obtained by NSSL. This anticyclonic storm formed when an echo, 150 nm south-southwest of NSSL, split shortly before 1430. A cyclonic echo with a life of less than three hours moved toward the 50° direction at about 20 kt, while the anticyclonic storm under discussion traveled toward the 20° direction with a speed in excess of 40 kt during its mature stage. The WSR-57 radar at NSSL followed this storm for about six hours until it disappeared to the north-northeast

of the radar.

When the topography of both top and base of the anvil extending from this cloud was mapped by using a series of RHI pictures taken at 4° -azimuth intervals (see Fig. 10), it was found that the anvil top, as well as the base, sloped up toward the direction of the storm motion. The south edge of the anvil was only 15,000 ft high, but its northern edge was over 30,000 ft, resulting in the shape of a tilted roof. Of interest is a CAPPI presentation of the anvil (see Fig. 11) constructed from contour lines in Fig. 10. The area of the anvil intersected at 20,000 ft was seen to the south of that at the 35,000 ft, without overlapping. The vertical cross-section of the hard-core portion of the echo along the line PQ is presented in Fig. 10. The hatched area designates -12 db or brighter echo obtained from RHI pictures. Near the surface, an area of -36 db echo is seen to the southeast of Fort Sill, which is located directly beneath the highest top of the RHI echo extending to 55,000 ft.

The anvil top reached only 37,000 ft as shown in the right diagram of Fig. 10. The vertical cross-section of the anvil at its source region suggests that the hydrometeors inside the anvil at 20,000 ft left the southern half of the cloud while those inside the anvil at 35,000 came from the northern half of the cloud. This feature of the anvil and the erosion mechanism previously discussed permit us to construct a tilted flow of undiluted air into this cloud. The flow is accompanied by an anticyclonic circulation. Successive arrows in the figure designate an updraft rising through the undiluted air to the anvil top, where the draft overshoots to about 55,000 ft. Thereafter the updraft changes into a downdraft descending to the anvil level or into an intense downdraft reaching the surface, where it spreads out. The spreading downdraft was characterized by an anticyclonic absolute circulation.

6. Numerical Model of Split Thunderstorms

We may enumerate the characteristics of split thunderstorms discussed in the previous section as follows:

1. An initial echo very abruptly splits into two, forming a pair of echoes.

2. The echo to the right veers to the right as much as 30°, and its traveling speed decreases.

3. The echo to the left veers to the left as much as 50°, and its traveling speed increases.

4. The surface winds beneath these right- and left-veering storms are cyclonic and anticyclonic, respectively.

5. The anvil orientation of the cyclonic storm is very close to the direction of the storm, but the anvil of the anticyclonic storm extends almost 90° to the right of the storm's direction, thus forming a converging anvil when both storms are in their mature stage.

6. These split storms form a counterpart couplet, but they are not mirror images of each other.

7. The initial echo before a split may be neutral or rotating and a split echo may split again.

We shall now try to find out if some of the numerically produced 1008 model clouds simulate a couplet of split thunderstorms. From the above-mentioned characteristics, it is natural to select a cyclonic storm and its anticyclonic counterpart as a couplet. The parameters thus chosen are:

High shear case: 100 kt -240°
Maximum vertical velocity: 15 m/sec
Inflow diameter: 20 km
Rotational Speed: +5 m/sec for cyclonic and -5, for anticyclonic storm

The diameters and rotational speeds[4] for these storms computed from Eqs. (18) and (22) give a diameter of 10 km and a rotational speed of 8 m/sec at the 6-km level.

Fig. 12 shows the counterpart couplets thus produced numerically. In determining the shape of the cloud depicted by discs at various heights, the positions of a rising disc were moved in the direction opposite from the inertia velocity the same distance as that traveled by the cloud during the time taken for the disc to ascend from the cloud base to each height. These positions were computed at 100-m intervals from the cloud base

---

[4] Computed values of D and V and input winds, W.

Height	1.5	2.0	3.0	4.0	6.0	8.0	9.0	10.0	11.0	11.5 km
Diameter	20.0	17.4	14.2	12.4	10.7	11.1	12.3	14.9	21.6	31.3 km
Rot. Speed	5.0	5.7	6.8	7.5	8.1	7.3	6.3	5.1	3.4	2.3 m/s
W (direction)	160	192	214	222	231	237	239	239	240	240 deg
W (speed)	16	25	39	47	61	78	85	92	96	98 kt

upward. The orientation of the anvils was obtained by first eroding the edge of the undiluted cloud and then drifting the eroded particles horizontally with the relative wind between the environmental winds and the inertial velocity of the cloud.

The coincidence between the numerical model and the observed split couplets turned out to be quite remarkable, since the model clouds explain most of the seven characteristics of split thunderstorms except No. 1, the reason why a thunderstorm splits into two in the first place.

Presented in Fig. 13 is a radar photograph of an echo couplet of April 23, 1964. The combination of antenna elevation and distance would result in an intersection of the radar beam and the echo at about 18,000 ft. When the anvil pattern in the photograph is examined, it is seen that the two anvils extending from these echoes are oriented in converging directions. A comparison of this photograph with the shape of the anvils at 6 km of numerically produced clouds in Fig. 12 reveals a striking similarity. Radar photographs taken prior to 1649 CST showed that echo couplets were formed earlier when an echo split suddenly into two. Thereafter, the one on the north veered to the left and the other, on the south, veered to the right. The numerically produced cloud couplet in Fig. 12 was obtained by adding cyclonic and anticyclonic circulations to a pair of clouds initially located close to each other. Since the location, shape, and anvil orientation of radar echoes and those of model clouds are very similar, it would be reasonable to assume that the left-veering echo represents an anticyclonic storm and the right-veering echo, a cyclonic storm. This result implies that storms within a small area may move in different directions if their circulations are considerably different from each other.

In order to generalize the velocity of cyclonic and anticyclonic storms of varying diameter and rotational speed, the inertial velocities computed from Eq. (23) were contoured in Fig. 14. The storm couplets under discussion were assumed to be D_o = 20 km and V_o = 5 m/sec. The computation, however, covered a range of V_o between -10 and +10 m/sec and of D_o up to 40 km. Contour lines of the inertial speed clearly indicate that an anticyclonic storm travels much faster than its counterpart cyclonic storm. This seems to be true in practically all ranges of D_o and V_o .

Of extreme importance are the veering angles of rotating storms. The computation revealed that the maximum left deviation occurs when the rotational speed is between 2 and 3 m/sec. If a cloud rotates anticyclonically faster than this critical rotation rate, the deviation gradually decreases. A similar phenomenon is also seen in cyclonic storms. For them, the critical rotation rate increases from 6 to 10 m/sec as the cloud diameter increases. This new evidence brings up a significant question as to

why a cloud does not deviate more when it rotates faster, for the conditions considered.

Another striking fact seen in Fig. 14 is the effect of the cloud diameter on the direction of the storm motion. Contrary to the expectation that the larger the storm the more it deviates to the right, the figure clearly indicates that the larger the storm, the less it deviates to the right. Moreover, a neutral storm travels from a direction ranging between 205° and 185°, which is considerably to the left of 215° (700-mb wind) and 225 (500-mb wind) directions. The mean wind averaged throughout the cloud depth is 220°.

Newton and Fankhauser's (1964) empirical results reveal that large echoes travel definitely to the right of the mean tropospheric wind and that the deviation increases with the storm diameter. Their finding is contradictory to this numerical result unless we increase the diameter along a line of constant vorticity instead of a line of constant rotational speed.

Let us now assume that the subcloud air converges into the cloud base while conserving its absolute angular momentum, and write

$$V_s R_s + \tfrac{1}{2} f R_s^2 = V_o R_o + \tfrac{1}{2} f R_o^2 , \qquad (27)$$

where suffixes s and o refer to "subcloud layer" and "cloud base," respectively. Replacing the radius, R, by the diameter, D, we divide both sides by D_o^2 to obtain

$$C^2 \zeta_s + C^2 f = \zeta_o + f ,$$

where $\zeta_s = 4V_s/D_s$, $\zeta_o = 4V_o/D_o$, and $C = D_s/D_o$

are, respectively, the relative vorticity of the subcloud layer, that of the inflow air at the cloud base, and the diameter reduction of the subcloud air before reaching the cloud base. The relative vorticity at the cloud base is thus expressed by

$$\zeta_o = (C^2 - 1) f + C^2 \zeta_s . \qquad (28)$$

This equation indicates that the vorticity at the cloud base is several times larger than that inside the subcloud layers. If we assume that the inflow diameter decreases to one-half before condensation takes place, Eq. (28) is reduced to

$$\zeta_o = 3f + 4\zeta_s . \qquad (29)$$

The relative vorticity within a synoptic scale cyclone is usually in excess of $5 \times 10^{-5} sec^{-1}$, and the magnitude of f is about $9 \times 10^{-5} sec^{-1}$, at the cloud base. It may be postulated that the relative vorticity inside the undiluted air at the cloud base is

not affected by the diameter, D_o, so long as ζ_s and C remain unchanged. As a result, an increase in the cloud-base diameter takes place not under V_o = const. but under ζ_o = const.

The isolines of ζ_o in a D_o vs V_o diagram such as that in Fig. 14 naturally form a group of straight lines radiating from a point where $D_o = V_o = 0$. If we assume that a cloud diameter increases while $\zeta_o = 50 \times 10^{-5}\text{sec}^{-1}$, the cloud would deviate only a few degrees to the right of the mean wind, the deviation being practically independent of the diameter. In order to obtain the right deviation in excess of 10°, the cloud-base vorticity must be between 50 and $100 \times 10^{-5}\text{sec}^{-1}$. In such a case, the cloud deviates more to the right, with an increasing diameter.

If a cloud develops over a region of zero relative vorticity, it would deviate more than 10° to the left. The fact that such a deviation is rare suggests that most of the thunderstorms with a large diameter, intense updraft, and strong environmental shear develop in a region of cyclonic subcloud vorticity and consequently rotate cyclonically.

7. Splitting Mechanism and Echo Motion after Split

We shall now postulate a reasonable mechanism of a thunderstorm split. A split usually takes place not too long after the appearance of the first echo, suggesting that it occurs approximately when the first gust line, as defined by Byers and Braham (1949), forms beneath the echo.

Recent investigation of the mid-tropospheric flow around mature thunderstorms shows a marked split in the flow of ambient air, creating wake flows trailing behind convective towers. Schematical views of a thunderstorm in this stage appear in Steps 1 and 2 in Fig. 15. The vortices, symmetric or random, left in the wake, drift away with a velocity similar to that of the ambient flow. There is no significant relative velocity between the translational motion of these vortices and the ambient flow.

In Step 3, however, the first gust line moving just beneath a pair of vortices creates forced updrafts which transport the momentum of the subcloud air up to the level of these vortices. This injection of low-level momentum into the vortex cores results in an immediate slow-down in the drifting speed of these vortices, initiating significant relative velocity between vortices and ambient flow.

As shown in Step 4, the Magnus lift force, which is proportional to the product of the circulation and the relative speed, begins to pull the vortex centers in such

a manner that the distance between them increases with time.

Because each storm grows to a large size, producing downdraft and precipitation, a mesoscale wind-shift line beneath each storm tends to travel with the storms. Step 5 shows the stage when two wind-shift lines, connected by a dissipating meso-front, are located beneath the clouds rotating in opposite directions. The initial storm, N, is dissipating rapidly due to the low-level divergence created by the development of a new storm couplet.

In order to evaluate numerically the characteristics of these counterpart storms, it was assumed that the storms, upon split, are characterized by the circulations, $\pm\Gamma_0$, which remain constant during the time when the cloud-base diameter increases from 15 to 30 km (see Fig. 16). We may call this the "growing stage." After the cloud-base diameter reaches a maximum, we assume that the diameter decreases to zero following the lines of constant vorticity of the subcloud layers. The split-echo cycles in Fig. 16 are superimposed upon Fig. 14, which gives the direction and speed of the inertia velocity of a given storm. Assuming also the linear change in the cloud-base diameter, the inertia velocities were obtained as a function of time.

The successive cloud positions thus plotted in Fig. 17 show a striking resemblance to the paths of the split storms of April 3, 1964 (Fig. 7). The life of the actual storms was not long enough to complete an "S-shaped" track of the anticyclonic storm and a "backward S-shaped" track of the cyclonic storm. Nonetheless, the pattern and speed of the actual storm are so similar to those computed theoretically that future refinement of the numerical experiment can be expected to solve various problems related to echo split and echo motion.

8. Review of the Effect of the Kutta-Joukowsky Force upon the Deviation of Storm Motion

The computer results, indicating that the deviation of both cyclonic and anti-cyclonic storms reaches a maximum value with a critical rotational speed of only a few meters per second, present an interesting but paradoxical problem. Why does the cloud motion not deviate more with increasing rotational speed?

In order to visualize the angle of deviation, a numerical experiment was performed by simulating a case where westerlies of constant direction (270°) but of two variable speeds (50 kt and 100 kt) act as the steering flow above the cloud base up to the cloud top. The inflow wind at and below the cloud base was assumed at 20 kt from 170°. The rotational speeds of the inflow air at the cloud base were

changed from -15 to +15 m/sec at intervals of one meter per second. A combination of two vertical shears, three vertical velocities, four diameters, 31 rotational velocities, and 18 inflow directions produced a total number of 13,392 inertial velocities.

Since most of the echo-split cases occurred when the inflow direction was between 135° and 180°, measured clockwise from that of the mean tropospheric winds, analyses in Fig. 18 and 19 were made for the inflow direction of 170°. The effects of vertical velocity upon the inertial speed, while keeping the vertical shear and the inflow diameter constant, are such that the larger the vertical velocity, the slower the inertial speed within practically the entire range of the storm's rotation. The minimum inertial speed, occurring when a storm rotates less than one meter per second cyclonically, increases with the rotation speed, which may be either cyclonic or anticyclonic. The direction of motion does not deviate more than 10 m/sec when the vertical velocity is smaller than 5 m/sec. As the vertical velocity increases, however, the right deviation of cyclonic storms and the left deviation of anticyclonic storms become significant. There is a critical value in the rotational speed giving rise to the maximum deviation of cyclonic or anticyclonic storms. This critical rotational speed is only a few meters per second, beyond which the deviation decreases in an oscillatory fashion. For all ranges of the vertical velocities, a storm deviates up to 10° to the left.

The effects of vertical shear do not significantly change the inertial speed divided by the steering wind speed, except for a slight shift of the minimum inertial speed toward the cyclonic side. The right deviation of cyclonic storms increases slightly with decreasing wind speed, but the left deviation increases 20° to 38° when the wind speed decreases from 100 to 50 kt. Even a non-rotating storm deviates about 35° to the left, thus necessitating a 1.4-m/sec cyclonic rotation in order not to deviate a storm with D_o = 20 km and w_{max} = 10 m/sec traveling inside a 50 kt westerly wind. The critical rotational speed resulting in a 38° left deviation is only -1.8 m/sec.

The effects of inflow diameter are more complicated than those for which empirical rules have been established so far. The numerical results indicate that a non-rotating storm deviates to the left almost in proportion to the diameter, and that a cloud must rotate faster in order not to deviate when the diameter increases. Furthermore, a cloud must rotate faster than about 3 m/sec in order to deviate more to the right with an increasing diameter. The inertial speed decreases considerably

with an increasing diameter, resulting in only 20% of the wind speed when D_o = 40 km and the cyclonic rotational speed is 2 m/sec.

As shown in this example, it is almost impossible to estimate within a 10° accuracy the deviation of a storm with varying diameter, vertical speed, vertical shear, and inflow velocity. Nevertheless, it will be feasible to establish several rules regarding storm velocities when complete cause-and-effect analyses are completed with the aid of electronic computers.

9. Summary and Conclusions

The observational and theoretical background leading to the development of the new concept of storm motions presented in this paper was accumulated during the past few years since the National Severe Storms Project was established in Kansas City. First of all, the airborne measurements of Doppler winds, that underwent complete error analysis in cooperation with the Research Flight Facilities, permitted the authors to construct reasonable airflow patterns around mature thunderstorm cells. During the past two years, especially, the authors made a number of flights with RFF's DC-6Bs over the Oklahoma-Kansas area in an attempt to gather wind, photographic, and airborne radar data necessary for the establishment of the numerical experiments presented herein. The latest development of weather radar facilities at the National Severe Storms Laboratory provided the opportunity for studying the three-dimensional features of thunderstorms with peculiar shapes, motions, and behavior, stimulating the authors' interest in these peculiarities photographically recorded by the Laboratory.

Unlike the conventional, empirical approach in establishing possible rules of echo motion, the authors started from gradient, Coriolis, drag, and lift forces acting upon undiluted incloud air rising through a circular cloud base. Taking the effect of entrainment into consideration, the horizontal displacement of steady-state rising air inside the undiluted core was obtained through the step-by-step integration from the base to the top of the cloud through over 100 steps. By using environmental conditions similar to those observed on April 3, 1964 when several splits occurred and by changing various parameters, a total of 1008 clouds was obtained.

A comparison of these clouds with actual split-echo couplets revealed that the appearance as well as the directions and speeds of these echoes are almost identical to those obtained numerically.

Discussed also in this paper are the effects of the Kutta-Joukowsky force upon the deviation of cloud motion. It was found that the deviation reaches a maximum when a storm, cyclonic or anticyclonic, rotates at only a few meters per second. If a cloud rotates faster than the critical rotational speed, the deviation decreases, contrary to the expectation that the faster the rotation, the larger the deviation.

Another interesting finding is that a cloud with a large diameter deviates to the left of the mean wind. Consequently, a cloud must rotate slowly and cyclonically in order not to deviate to the left. A theoretical estimate, under the assumption of the conservation of absolute angular momentum, indicated that most thunderstorms tend to rotate, due to the fact that they develop on the rotating earth. The cyclonic relative vorticity in the subcloud layers gives additional rotation.

Since the above-mentioned conclusions refer to a limited set of initial and environmental conditions, further numerical model experiments are being made at SMRP in order to generalize the velocities of thunderstorms. It is expected that the echo motions in relation to various environmental and cloud parameters will be investigated through more sophisticated simulation of thunderstorm circulation involving up- and downdrafts.

Acknowledgements:

The authors are very grateful to the staff members of NSSL, who obtained radar pictures and made them available to the authors and who also contributed valuable comments during discussions. Appreciation should also be extended to those who operated the Beta Network from which valuable information on low-level winds was obtained. The aircraft measurements by RFF's DC-6Bs contributed significantly to the determination of flow patterns around convective towers. The programming for the University of Chicago's 7094 computer was done by Gisela Baralt of SMRP, who participated in the improvement of the authors' numerical experiments.

APPENDIX I

Influence of Entrainment upon Cloud Diameter and Storm Motion

In the numerical experiments presented in this paper, the entrainment coefficient, k_z, defined by Eq. (16) was assumed to be 0.4. The cloud diameters were then computed from Eq. (19). There could, of course, be some question as to what would happen if other values are used as the entrainment coefficient.

Computations were performed using three different values of k_z, namely, 0.0, 0.4, and 0.8. It was revealed that the undiluted core disappears at an altitude of about 9 km when $k_z = 0.8$ is used for a cloud with a base diameter of 5 km (see Fig. A1). As the cloudbase diameter, D_o, increases, the influence of the entrainment coefficient upon the cloud diameter becomes less significant. Severe storms, which usually have a diameter, D_o, larger than 20 km, remain practically unaffected even if the entrainment coefficient is increased to 0.8, which is twice as large as the value used in this paper.

The influence of entrainment upon the inertia velocity of storms was evaluated by using the cyclonic ($V_o = +5$ m/sec) and the anticyclonic ($V_o = -5$ m/sec) storms shown in Fig. 12, which was obtained by using $D_o = 20$ km and $W_{MAX} = 15$ m/sec as input data. The direction and speed of both storms appear in Fig. A2 in which D_o, in both kilometers and miles, increases upward from 0 to over 40 km. If we arbitrarily classify convective clouds into small cumuli, large cumuli, small storms, and large storms, as shown schematically in Fig. A2, most of the hail- and/or tornado-producing thunderstorms are included in large storms. It is seen that the direction of movement of these large storms varies only up to a few degrees when the entrainment coefficient is changed as much as ± 0.4 from $k_z = 0.4$, the value used in this paper. The change in storm speed within this range of k_z is also no more than a few knots, thus suggesting that the storm velocities computed by assuming $k_z = 0.4$ are representative of those of large storms. For small storms and cumulus clouds, the influence of the entrainment coefficient upon the storm speed is so large that it is not feasible to estimate their motion without knowing the coefficient more accurately.

APPENDIX II

Shape of the Model Clouds

After computing the disc diameters as a function of height, the three-dimensional trajectory of a disc center was computed starting at the cloud base. If we assume that the initial conditions of cloud and environment do not change, then successive discs will follow the same trajectory with respect to their location at the cloud base. The shape of a cloud is the boundary of stacked discs at a given fixed time. If the cloud base remains stationary, the cloud axis will be identical to the trajectory of the disc center, as in the case of rising smoke from a large circular chimney. If the cloudpropagates, its axis no longer coincides with the trajectory of the disc center. Figure A3 shows that the propagation of the vertical motion field at the cloud base reduces the tilt of the cloud axis considerably, while the trajectories of the disc centers remain unchanged. The numbers by the black points on the trajectories are the relative times for the disc centers measured from their crossing of the cloud axis at $t = 0$, as appears in the figure. It should be noted that the shape of the cloud axis, as well as that of the model cloud as a whole, remains unchanged while it propagates from left to right. Nevertheless, the velocity of each stacked disc forming the cloud varies as a function of height; that is, the upper discs move much faster than the lower ones. The cloud, however, maintains its shape regardless of such differential motion of the discs. The cloud base in the figure was moved from left to right at the inertia velocity, $\bar{\mathbf{S}}$, assuming that the propagation of the vertical motion field at the cloud base is equal to the inertia velocity of the model cloud.

Presented in the lower half of Fig. A3 are the velocity hodographs of anticyclonic, cyclonic, and neutral storms under the influence of the veering and shearing winds, which are indicated by the heights in km in the small square boxes. The vector of the inflow wind at the 1.5-km level is assumed to be SSE at 15 kt. When a storm does not rotate, the rising disc is accelerated downwind, due mainly to the drag force. Thus the relative winds and the acceleration of the disc at all levels are more or less in the same direction. When the storm rotates anticyclonically, the Magnus force effectively accelerates the rising disc toward the northwest at low level, the north at middle level, and the northeast at high level. A storm disc at high level may thus move much faster than any environmental wind. The Magnus force acting upon the cyclonic storm in the figure first reduces the disc speed at low level, thus resulting in rather slow storm motion compared with that of the anticyclonic storm. The figure also includes the inertia velocities, $\bar{\mathbf{S}}_A$, $\bar{\mathbf{S}}_C$, and $\bar{\mathbf{S}}_N$, of anticyclonic, cyclonic, and neutral storms, respectively. It is important to realize that relative winds between the inertia velocity of a storm and its environmental winds at various levels are fictitious ones which should not be used in determining dynamical interaction between clouds and their environment. The interaction must be computed from the motion of the disc relative to the wind at the same level, because the storm or disc velocity, $\mathbf{S}$, and the inertia velocity, $\bar{\mathbf{S}}$, could be quite different from each other.

REFERENCES

Bates, F. C., 1961: The Great- Plains thunderstorm - a model. Ph.D. dissertation, St. Louis Univ., 164 pp.

_____, and C. W. Newton, 1965: The forms of updrafts and downdrafts in cumulonimbus in a sheared environment. Paper presented at AMS, Reno Meeting.

Browning, K. A., 1964: Airflow and precipitation trajectories within severe local storms which travel to the right of the winds. J. Atmos. Sci., 21, 634-639.

_____, 1965(a): The evolution of tornadic storms. J. Atmos. Sci., 22, 664-668.

_____, 1965(b): Some inferences about the updraft within a severe local storm. J. Atmos. Sci., 22, 669-667.

_____, and T. Fujita, 1965: Comments on "Formation and steering mechanisms of tornado cyclones and associated hook echoes" and reply. Mon. Wea. Rev., 93, 639-643.

Byers, H. R., 1942: Nonfrontal thunderstorms. Dept. Meteor., Univ. of Chicago, Misc. Reps. No. 3, 22 pp.

_____, and R. R. Braham, 1949: The thunderstorm. Government Printing Office. Washington, D.C. 287 pp.

Fujita, T., 1958: Mesoanalysis of the Illinois tornadoes of 9 April 1953. J. Meteor. 15, 288-296.

_____, 1963: Analytical mesometeorology: A review. Meteorological Monographs Vol. 5, No. 27, 77-125.

_____, and J. Arnold, 1963: Preliminary result of analysis of the cumulonimbus cloud of April 21, 1961. SMRP Res. Paper 16, 16 pp. (Available from SMRP)

Fujita, T., 1965: Formation and steering mechanisms of tornado cyclones and associated hook echoes. Mon. Wea. Rev., 93, 67-78.

_____, 1966: Accurate calibration of Doppler winds for use in the computation of mesoscale wind fields. Mon. Wea. Rev., 94, 19-35.

_____, P. G. Black, and A. G. Loesch, 1966: Use of wet-beam Doppler winds in the determination of the vertical velocity of raindrops inside hurricane rainbands. SMRP Res. Paper 59, 32 pp. (Available from SMRP)

Fulks, J. R., 1962: On the mechanics of the tornado. NSSP, Rep. 4, 34 pp.

Harrold, T. W., 1966: A note on the development and movement of storms over Oklahoma on 27 May 1965. NSSL Rep. 29.

Humphreys, W. J., 1928: Physics of the air. McGraw-Hill Book Co., Inc., New York, 676 pp.

Ligda, M. G. H., 1953: The horizontal motion of small precipitation areas as observed by radar. M. I. T. Tech. Rep. 21.

Newton, C. W., and S. Katz, 1958: Movement of large convective rainstorms in relation to winds aloft. Bull. Amer. Meteor. Soc. 39, 129-136.

Newton, C. W., and H. R. Newton, 1959: Dynamical interactions between large convective clouds and environment with vertical shear. J. Meteor., 16, 483-496.

Newton, C. W., and J. C. Fankhauser, 1964: On the movement of convective storms, with emphasis on size discrimination in relation to water-budget requirements. J. Appl. Meteor., 3, 651-668.

Prandtl, L., and O. G. Tietjens, 1934: Applied hydro- and aeromechanics. 1957 Edition, Dover Publications Inc., New York, 311 pp.

Stout, G. E., and H. W. Hiser, 1955: Radar scope interpretations of wind, hail, and heavy rainstorms between May 27 and June 8, 1964. Bull. Amer. Meteor. Soc. 36, 519-527.

Wieselsberger, V. C., 1921: Neuere Feststellungen über die Gesetze des Flüssigkeits- und Luftwinderstandes. Physikalische Z., 11, 321-328.

Wilk, K. E., 1966: Motion and intensity characteristics of severe thunderstorms ttttt of April 3, 1964. NSSL Rep. No. 29.

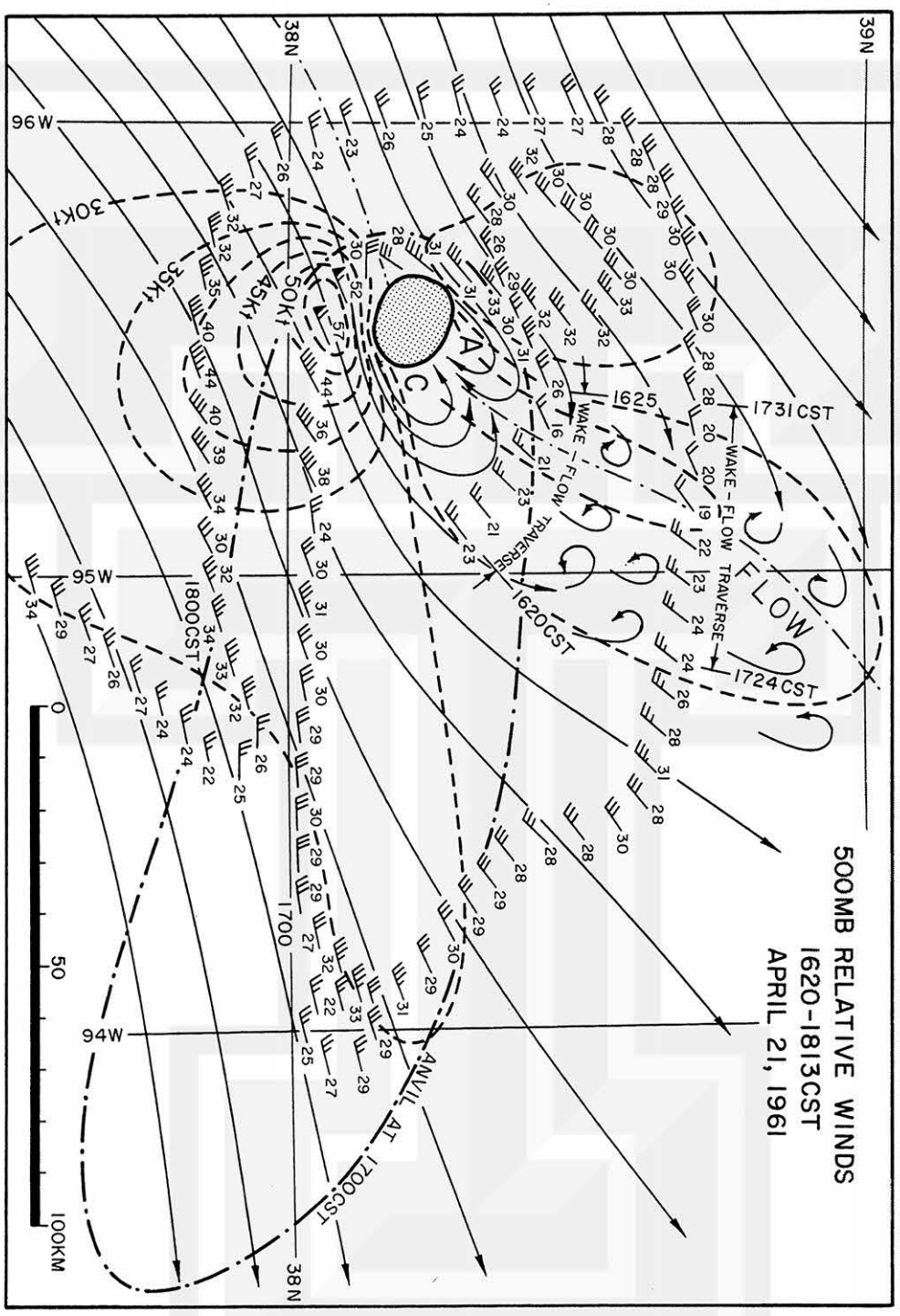

Fig. 1. Relative winds around a cumulonimbus of April 21, 1961 near Topeka, Kansas. Note that the axis of the wake flow is curved due to cyclonic circulation around the storm. Relative winds were obtained by subtracting the storm's velocity 268° - 22 kt from the Doppler winds measured by the DC-6B, 40C of RFF.

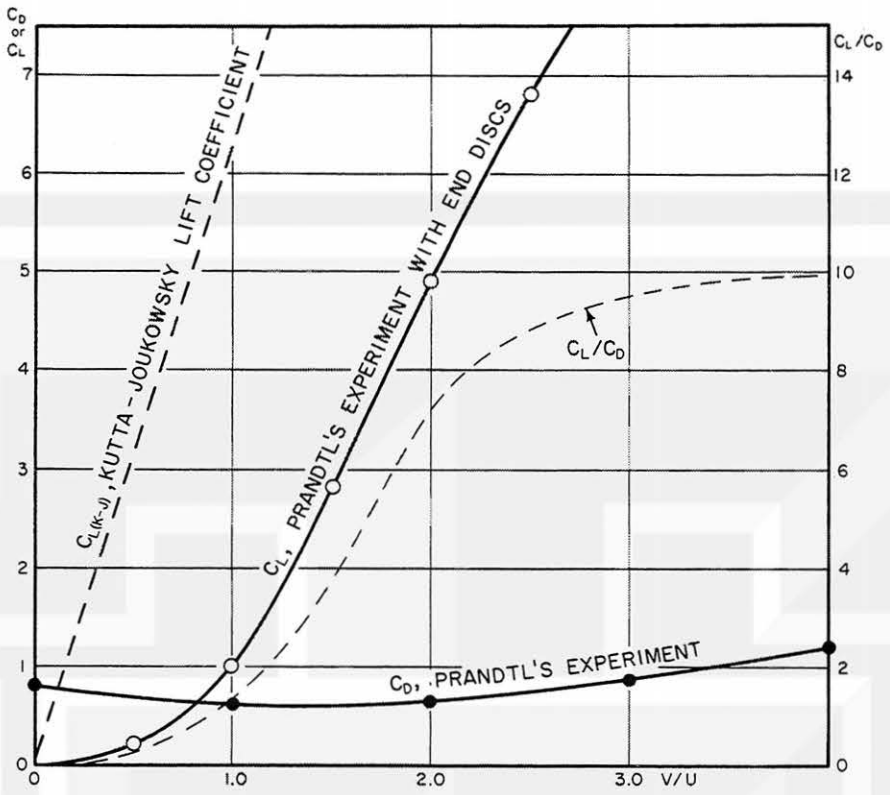

Fig. 2. Two lift coefficients, one from the Kutta-Joukowsky force and the other obtained by Prandtl (1934) through experiment by using a rotating cylinder with two end discs. The drag coefficient in the figure represents the value obtained through the same experiment.

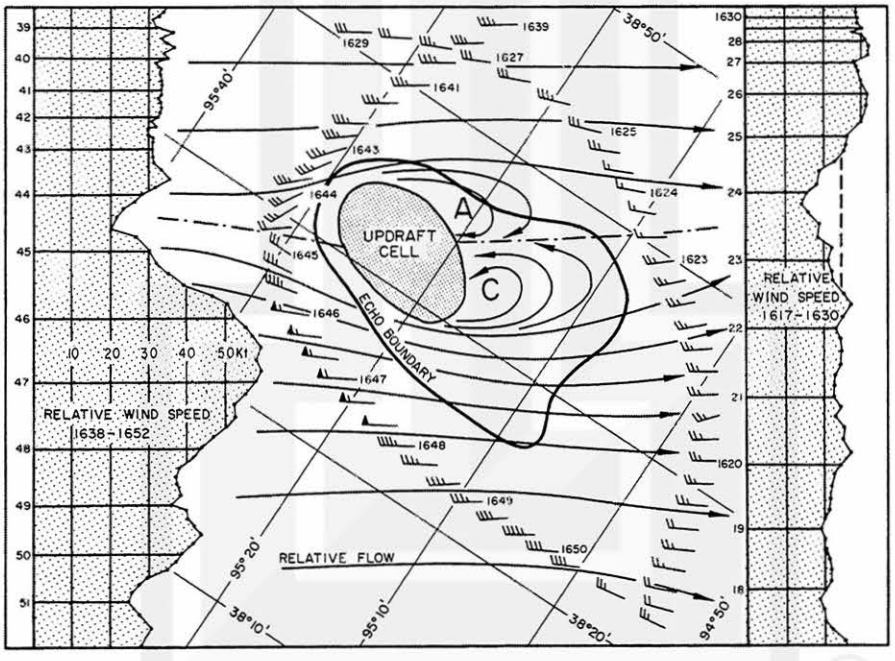

Fig. 3. An enlargement of the flow pattern around the cloud in Fig. 1. A similar vortex has been postulated by Fulks (1962) in an attempt to explain the mechanism of tornado formation. The upstream branches out near the forward stagnation point, and deficit flow speeds are noticeable in the wake region.

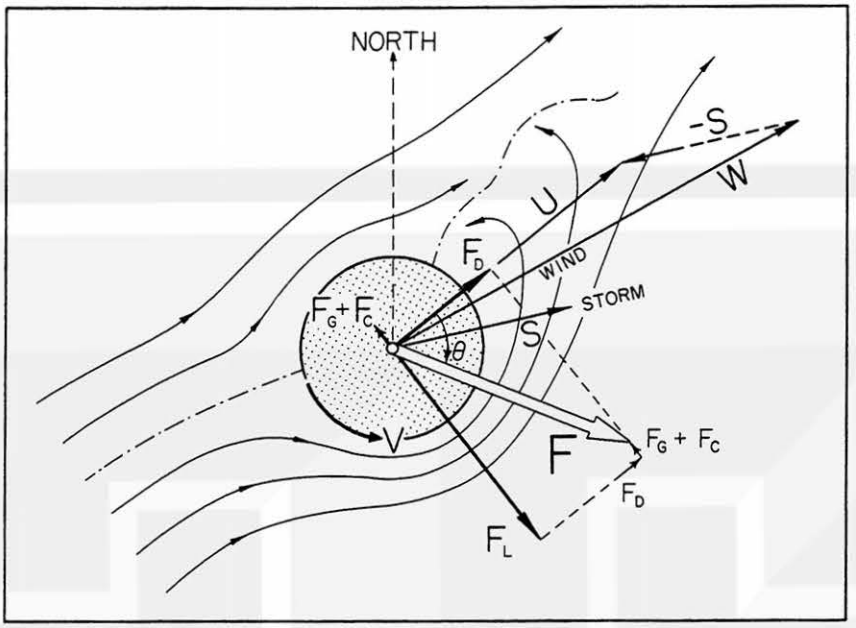

Fig. 4. Forces acting upon circular, rotating, incloud air which is assumed to be undiluted: the pressure gradient force, the Coriolis force, the drag force, and the lift force. The resultant force, designated by an open arrow, accelerates the undiluted air during the period when the air rises through a given vertical distance. S and U denote, respectively, the translational velocity of the undiluted air and the ambient flow velocity relative to S.

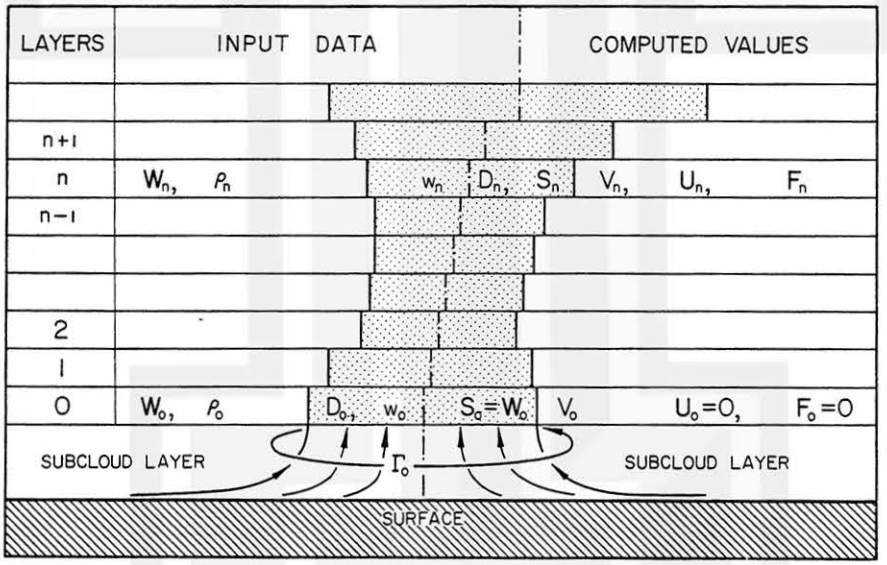

Fig. 5. Schematical diagram of a sliced cloud with circular cross-sections at all levels. For computation purposes, the thickness of each disc was selected as 100 m, thus establishing 105 layers between the cloud base at 1.5 km and the top at 12.0 km. The subcloud air was then brought in from the circular cloud base under a steady-state assumption. As the air rises, maintaining its circular cross-sections, the diameter shrinks to a minimum due to increasing vertical motion and erosion which overcome expansion by lowering the density. The cloud as a whole posesses a total horizontal momentum proportional to the inertia of the cloud system.

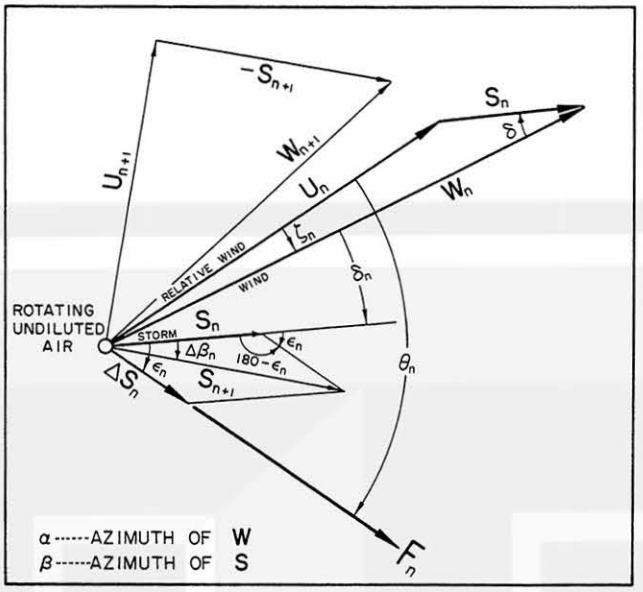

Fig. 6. Vector diagram used for step-by-step computation of horizontal velocities of incloud air. The notations are: W, speed of ambient flow with azimuth α; S, horizontal speed of the rising air with azimuth β; U, relative wind speed with azimuth γ; δ, azimuth of S measured from W; ΔS, acceleration due to the total force, F; ϵ, azimuth of ΔS measured from S; ζ, azimuth of W measured from U; θ, direction of the total force measured from the relative wind; and $\Delta\beta$, the change in the direction of the horizontal velocity of the undiluted incloud air while rising through the nth layer.

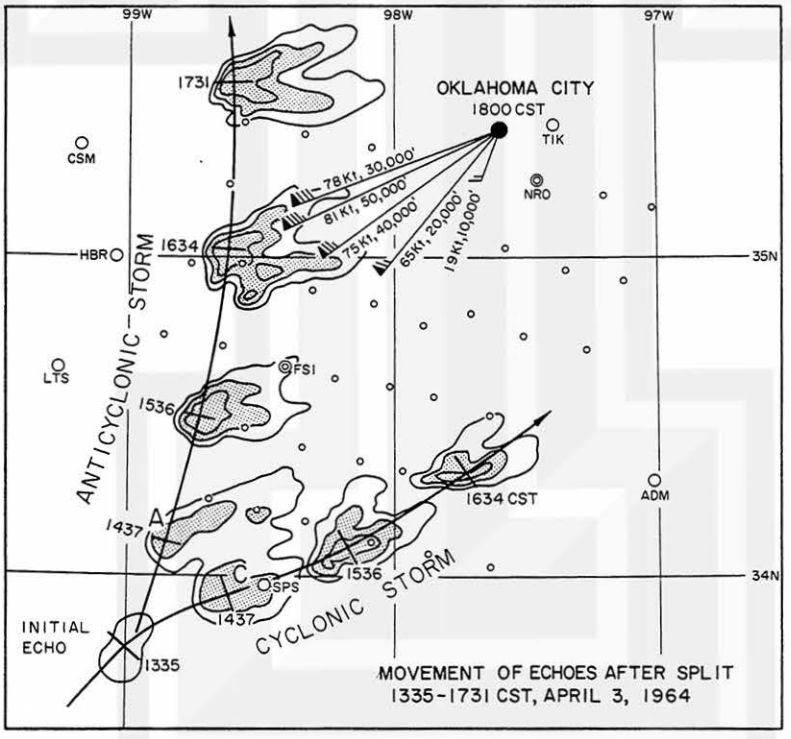

Fig. 7. Hourly positions and features of a split-echo couplet of April 3, 1964. For further information, refer to a paper by Wilk (1966). Similar split echoes were observed on April 23, 1964, and analyses of these echoes appear in Figs. 10, 11, and 13.

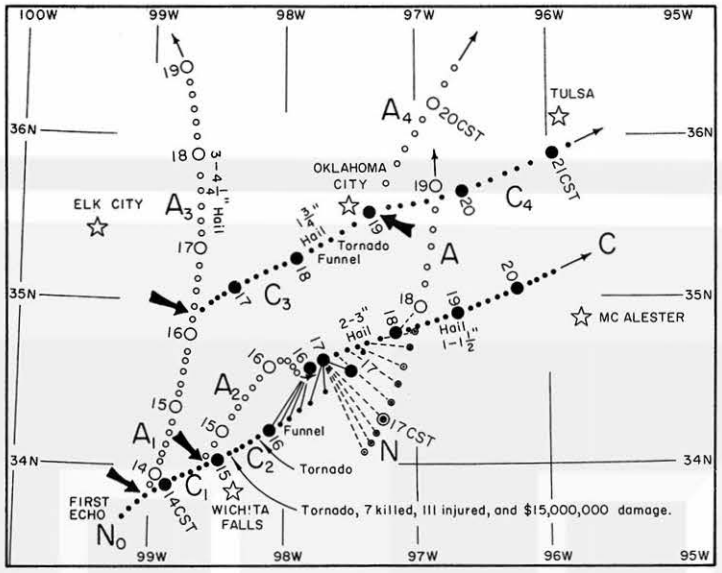

Fig. 8. Further splitting of the anticyclonic and cyclonic storms shown in Fig. 7. Open circles indicate anticyclonic storms; black circles, cyclonic. Cyclonic storm C_2, product of the second splitting, produced violent tornadoes, causing severe damage near Wichita Falls, Texas. Anticyclonic storm, A_3, also a second-split product, was characterized by 3- to 4 1/4-in hailstones.

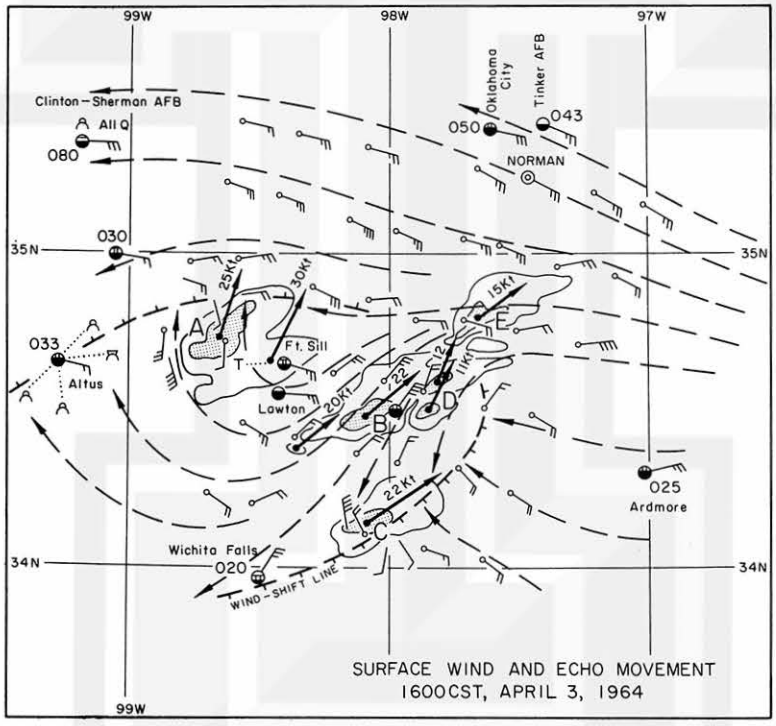

Fig. 9. Surface mesoanalysis of Beta Network wind data. Note that the cyclonic storm, C, and the anticyclonic storm, A, are accompanied, respectively, by cyclonic and anticyclonic circulations when integrated around closed circuits, including echo areas. Arrows indicate velocities of echoes, ranging between 11 and 30 kt in speed and between 10° and 60° in direction.

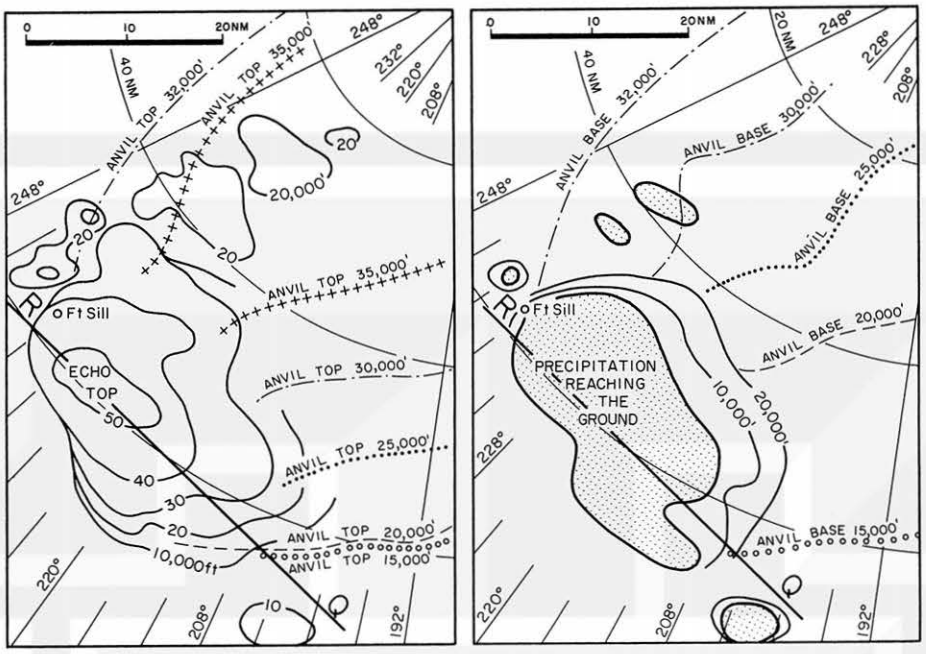

Fig. 10. Cloud-top (left) and cloudbase (right) topography of an anticyclonic storm of April 23, 1964. Contour lines for turrets and anvils are drawn for every 10,000 ft and 5,000 ft, respectively, using RHI photographs from Norman taken at about 1653 CST. Note that both anvil top and base slope up toward the north.

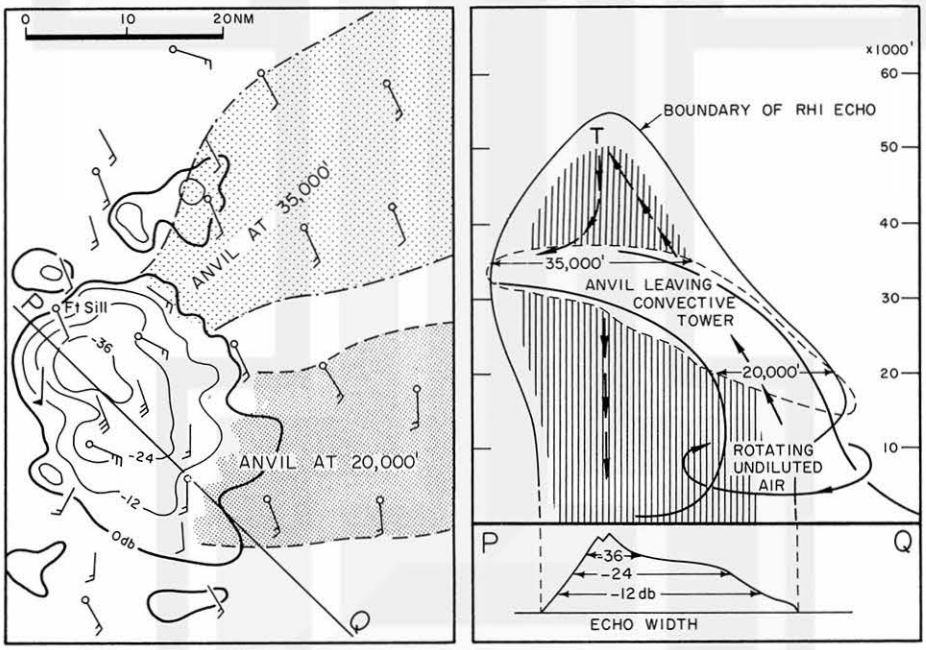

Fig. 11. Cross sections of the anvil at 20,000 ft and 35,000 ft obtained from the same RHI data used for the previous figure. The diagram to the right indicates the position of the sloping, rotating, undiluted air, estimated from the three-dimensional characteristics of the anvil under the assumption the anvil consists of eroded hydrometeors at various altitudes. Arrows indicate possible trajectories of up- and downdrafts

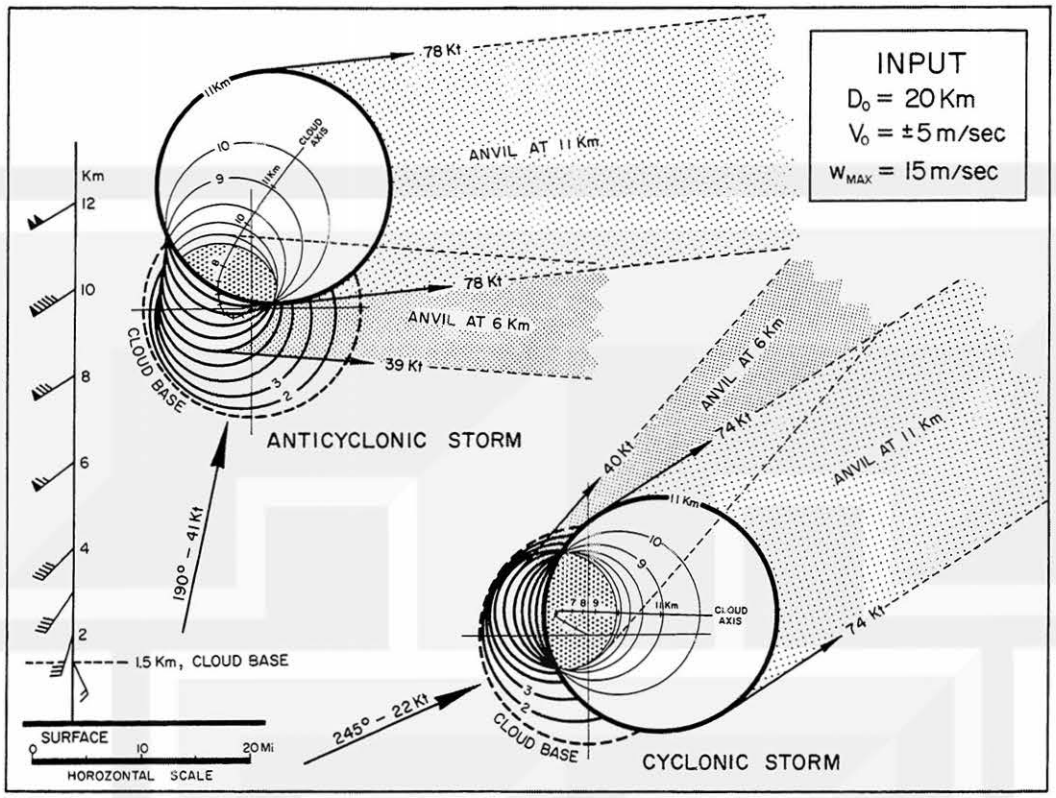

Fig. 12. A plan-view of a split-echo couplet, drawn entirely from computer output, with the following input data: ambient winds (shown to the left), 20-km cloud base diameter, ±5 m/sec rotational speed at the cloud base, and maximum vertical velocity of 15 m/sec. The computed inertial velocities of these two storms differ 55° in each direction and 17 kt in speed. The anvil directions seem to converge.

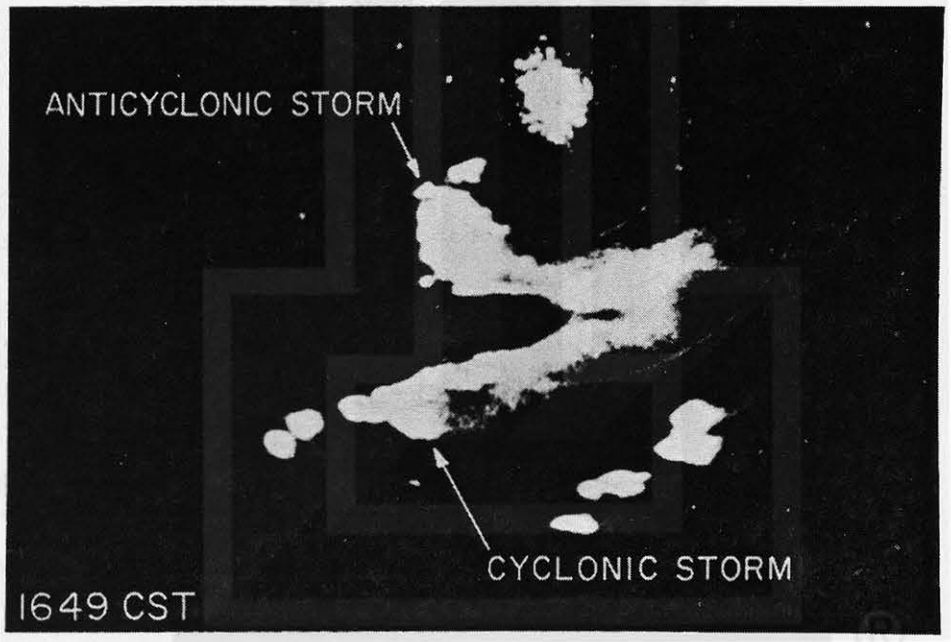

Fig. 13. An example of converging anvils from split storms of April 23, 1964. Range markers are 50 miles from the WSR-57 radar at Norman.

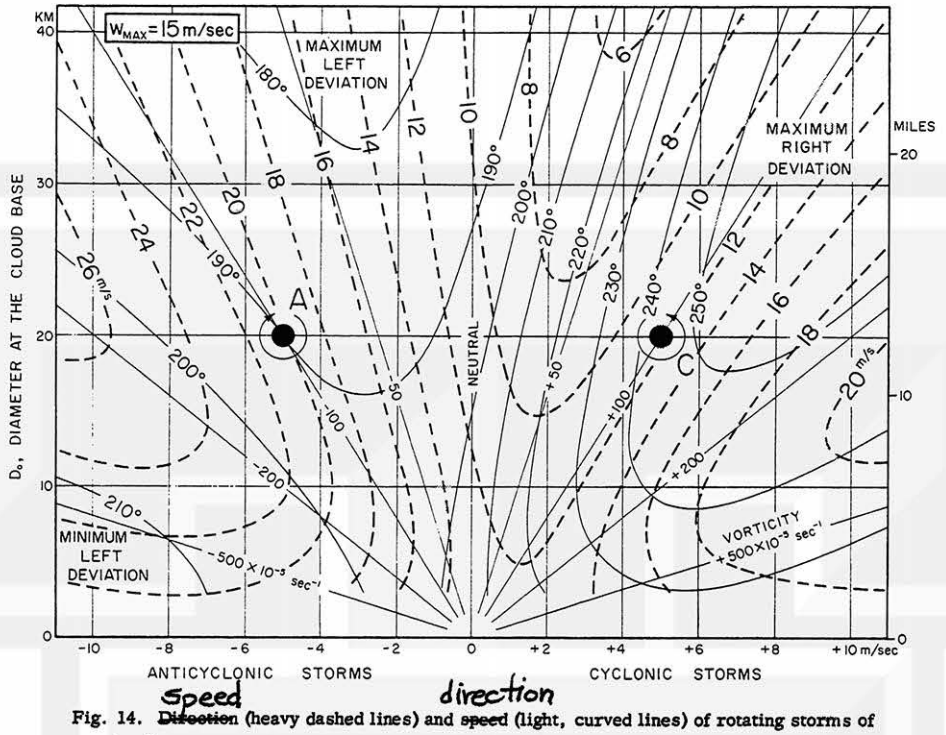

Fig. 14. ~~Direction~~ (heavy dashed lines) and ~~speed~~ (light, curved lines) of rotating storms of varying diameters, and rotational speeds. The straight lines radiating from the point of zero diameter and zero rotation denote the relative vorticity of the air rising through the circular cloud base.

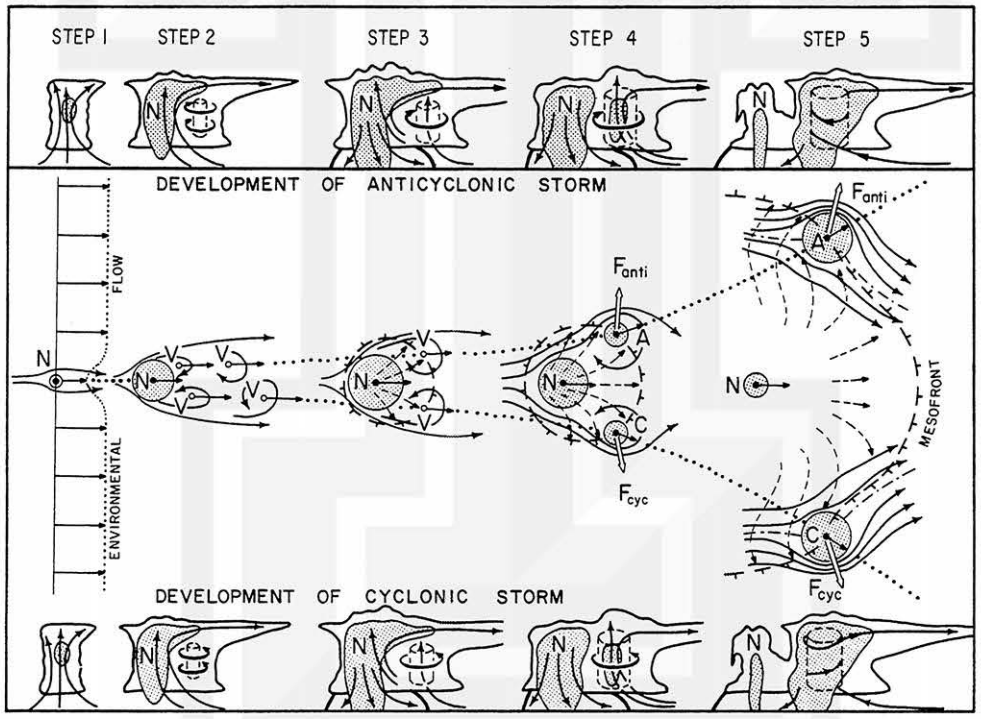

Fig. 15. Schematical diagram showing the steps in the process of storm splitting. The vertical cross-sections of the anticyclonic storm (top) and those of the cyclonic storm (bottom) are drawn so that they can be compared at each step with the plan-views shown in the middle.

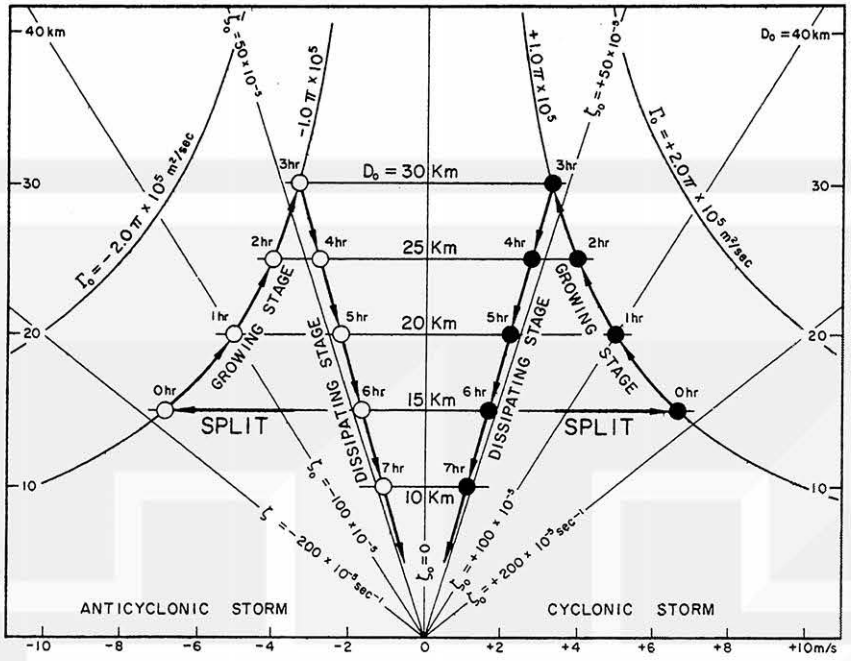

Fig. 16. Development cycle of a split-echo couplet drawn on diameter vs rotational speed coordinates. It is assumed that the diameter of the couplet increases in proportion to time, while conserving the circulation around each storm, and that this diameter decreases after reaching a maximum, again in proportion to time but while conserving the relative vorticity. The hyperbolic curves represent the lines of constant circulation.

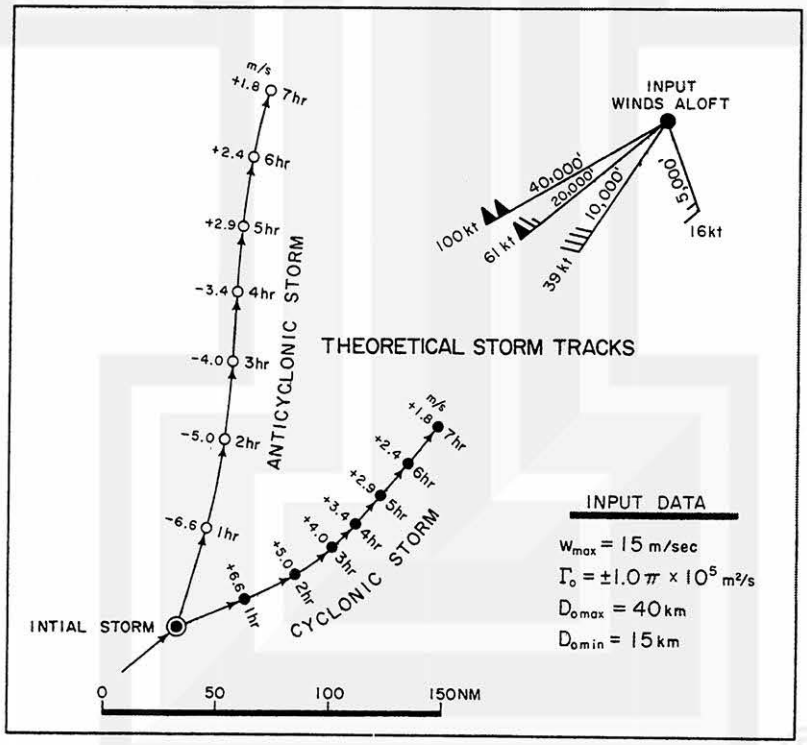

Fig. 17. Theoretical storm tracks obtained by computer, using the input data of Fig. 12 and the assumptions of Fig. 16. When this figure is compared with the observed storm tracks in Fig. 7, a remarkable coincidence can be seen.

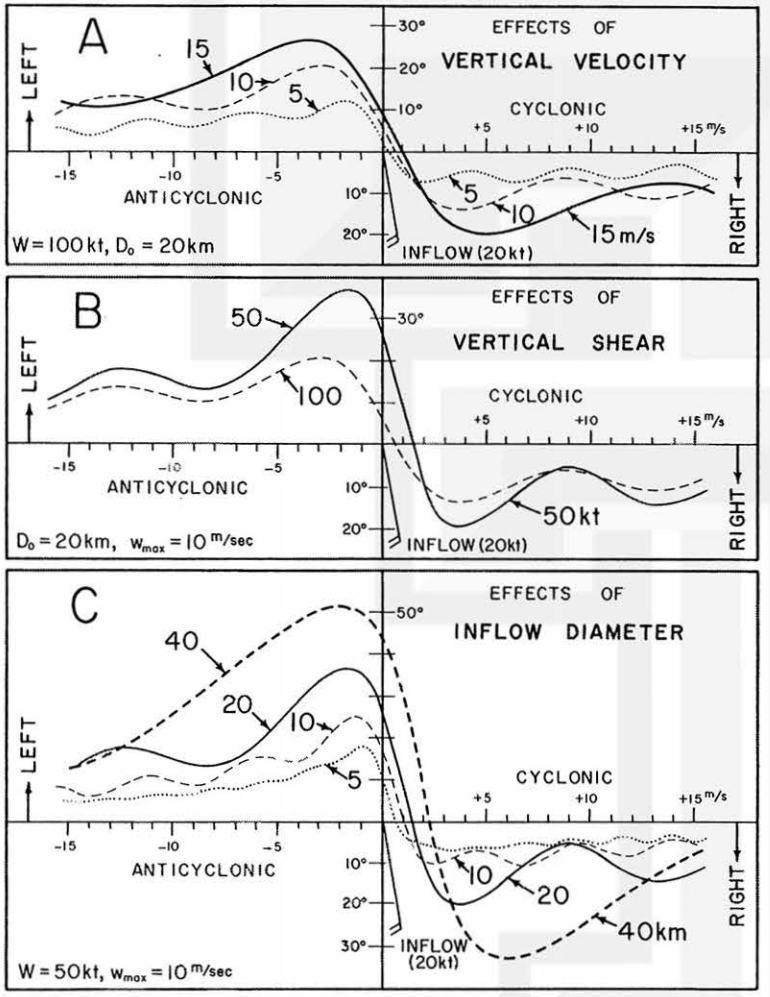

Fig 18. Diagrams showing the existence of critical rotational speeds at which the deviation of storms reaches a maximum. When a cloud rotates faster than the critical speed, the deviation, paradoxically, decreases in an oscillatory fashion.

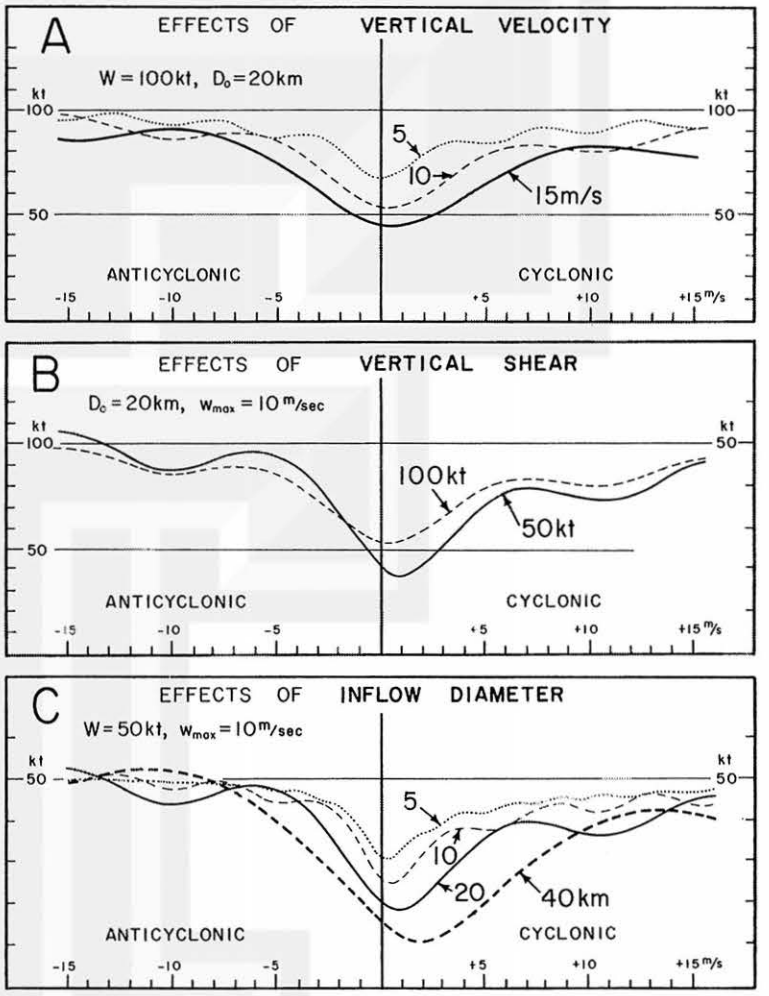

Fig. 19. Diagrams showing the change in inertial speed of storms when the vertical velocity, vertical shear, and inflow diameter are respectively varied, while keeping other parameters constant. Note that all storms move at approximately the speed of the environmental wind when their rotational speed is extremely high.

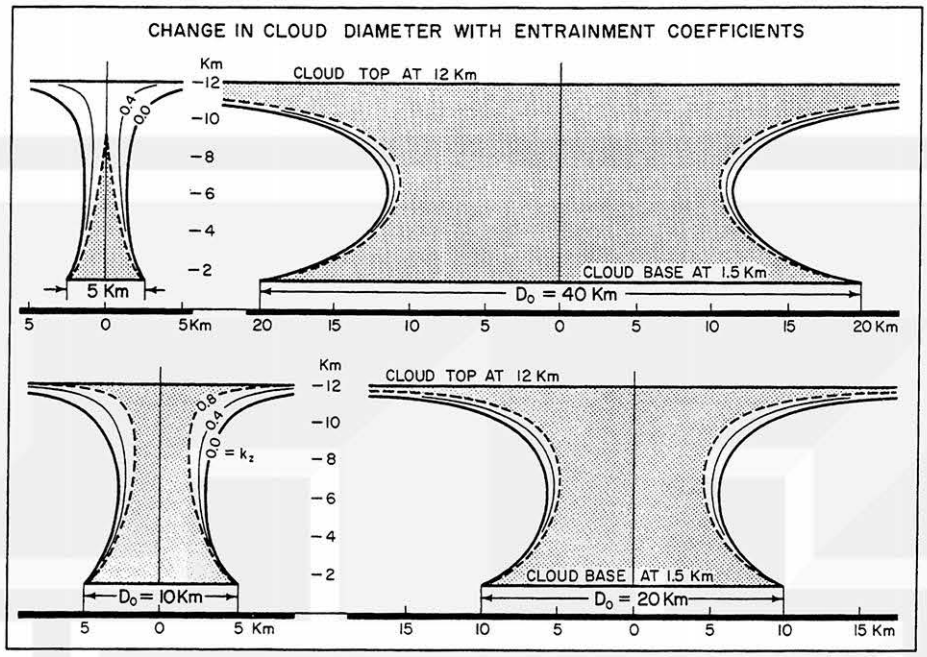

Fig. A1. Vertical variation of undiluted cloud diameter corresponding to entrainment coefficients, k_z = 0.0, 0.4, and 0.8. Note that these entrainment coefficients result in practically unique diameters of large storms.

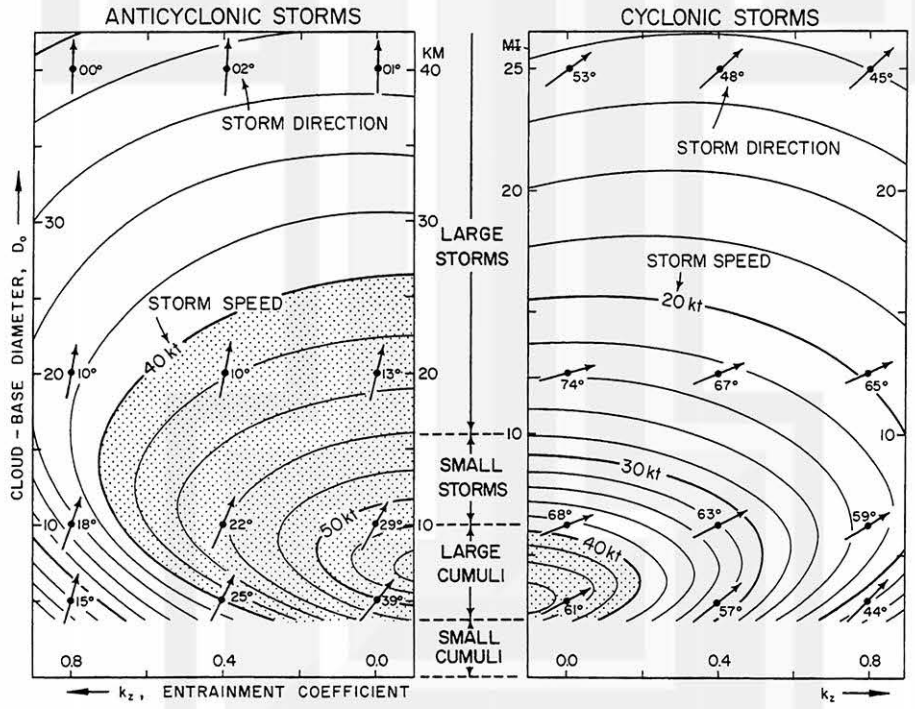

Fig. A2. Influence of entrainment coefficients upon the inertia velocity of anticyclonic and cyclonic storms (shown in Fig. 12). Both directions and speeds are shown on D_0 vs k_z coordinates. The effect of k_z, ranging between 0.0 and 0.8, upon large storms is negligibly small for all practical purposes. The regions of storm speed above 40 kt are stippled.

A3

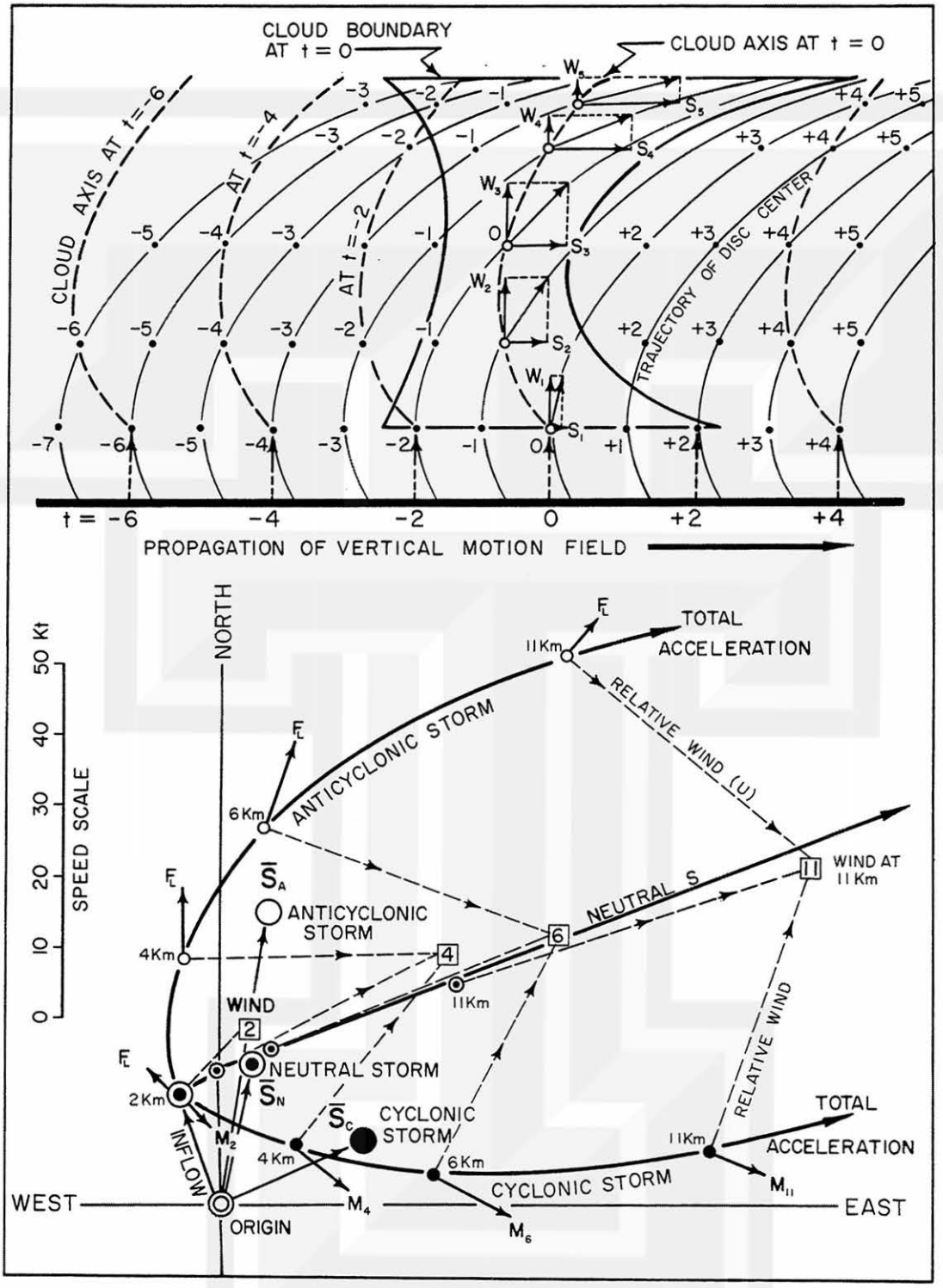

Fig. A3. Upper part: Relation of trajectory of disc centers and the shape of the cloud for a given value of propagation of vertical motion field. This propagation reduces the tilt of the cloud axis compared with that of the trajectory of the disc centers. Lower part: Velocity hodographs of anticyclonic, cyclonic, and neutral storms under the influence of veering and shearing winds. The Magnus force, perpendicular to the relative wind, is indicated by F_L.

MESOMETEOROLOGY PROJECT - - - RESEARCH PAPERS

(Continued from front cover)

42. A Study of Factors Contributing to Dissipation of Energy in a Developing Cumulonimbus - Rodger A. Brown and Tetsuya Fujita
43. A Program for Computer Gridding of Satellite Photographs for Mesoscale Research - William D. Bonner
44. Comparison of Grassland Surface Temperatures Measured by TIROS VII and Airborne Radiometers under Clear Sky and Cirriform Cloud Conditions - Ronald M. Reap
45. Death Valley Temperature Analysis Utilizing Nimbus I Infrared Data and Ground-Based Measurements - Ronald M. Reap and Tetsuya Fujita
46. On the "Thunderstorm-High Controversy" - Rodger A. Brown
47. Application of Precise Fujita Method on Nimbus I Photo Gridding - Lt. Cmd. Ruben Nasta
48. A Proposed Method of Estimating Cloud-top Temperature, Cloud Cover, and Emissivity and Whiteness of Clouds from Short- and Long-wave Radiation Data Obtained by TIROS Scanning Radiometers - T. Fujita and H. Grandoso
49. Aerial Survey of the Palm Sunday Tornadoes of April 11, 1965 - Tetsuya Fujita
50. Early Stage of Tornado Development as Revealed by Satellite Photographs - Tetsuya Fujita
51. Features and Motions of Radar Echoes on Palm Sunday, 1965 - D. L. Bradbury and Tetsuya Fujita
52. Stability and Differential Advection Associated with Tornado Development - Tetsuya Fujita and Dorothy L. Bradbury
53. Estimated Wind Speeds of the Palm Sunday Tornadoes - Tetsuya Fujita
54. On the Determination of Exchange Coefficients: Part II - Rotating and Nonrotating Convective Currents - Rodger A. Brown
55. Satellite Meteorological Study of Evaporation and Cloud Formation over the Western Pacific under the Influence of the Winter Monsoon - K. Tsuchiya and T. Fujita
56. A Proposed Mechanism of Snowstorm Mesojet over Japan under the Influence of the Winter Monsoon - T. Fujita and K. Tsuchiya
57. Some Effects of Lake Michigan upon Squall Lines and Summertime Convection - Walter A. Lyons
58. Angular Dependence of Reflection from Stratiform Clouds as Measured by TIROS IV Scanning Radiometers - A. Rabbe
59. Use of Wet-beam Doppler Winds in the Determination of the Vertical Velocity of Raindrops inside Hurricane Rainbands - T. Fujita, P. Black and A. Loesch
60. A Model of Typhoons Accompanied by Inner and Outer Rainbands - Tetsuya Fujita, Tatsuo Izawa, Kazuo Watanabe, and Ichiro Imai

MESOMETEOROLOGY PROJECT - - - RESEARCH PAPERS

(Continued from inside back cover)

61. Three-Dimensional Growth Characteristics of an Orographic Thunderstorm System - Rodger A. Brown.

62. Split of a Thunderstorm into Anticyclonic and Cyclonic Storms and their Motion as Determined from Numerical Model Experiments - Tetsuya Fujita and Hector Grandoso.